Localized activity patterns in excitatory neuronal networks

Jonathan Rubin* Amitabha Bose†

February 3, 2004

Abstract. The existence of localized activity patterns, or bumps, has been investigated in a variety of spatially distributed neuronal network models that contain both excitatory and inhibitory coupling between cells. Here we show that a neuronal network with purely excitatory synaptic coupling can exhibit localized activity. Bump formation ensues from an initial transient synchrony of a localized group of cells, followed by the emergence of desynchronized activity within the group. Transient synchrony is shown to promote recruitment of cells into the bump, while desynchrony is shown to be good for curtailing recruitment and sustaining oscillations of those cells already within the bump. These arguments are based on the geometric structure of the phase space in which solutions of the model equations evolve. We explain why bump formation and bump size are very sensitive to initial conditions and changes in parameters in this type of purely excitatory network, and we examine how short-term synaptic depression influences the characteristics of bump formation.

Short title: Localized activity patterns in excitatory networks

AMS Subject Classification: 34C15, 34D15, 37G15, 92C20

*Department of Mathematics and Center for the Neural Basis of Cognition, University of Pittsburgh, Pittsburgh, PA 15260; rubin@math.pitt.edu

†Department of Mathematical Sciences, New Jersey Institute of Technology, Newark, NJ 07102; bose@njit.edu

1 Introduction

Oscillatory activity in neuronal networks is widespread across brain regions. An important goal of current research in neuroscience is to measure the degree of correlation between oscillations and behavior. In particular, sustained patterns of activity that are localized in space have been recorded in several experimental settings. These patterns, often referred to as bumps of activity, have been correlated with working memory tasks (reviewed in [21, 2]) orientation or feature selectivity in the visual system (see e.g. [10]), and activity in the head-direction system in mammals (reviewed in [20, 19]). Recently, there has been renewed interest in modeling bumps in a variety of settings and numerous theoretical models for bumps have been developed (some of which are reviewed, for example, in [7, 21, 2]).

A standard ingredient in the generation of activity bumps in model networks is a so-called Mexican hat synaptic architectural structure. In networks endowed with this synaptic structure, neurons effectively send excitation to nearby neurons and inhibition to far away neurons. This setup allows excitation to build locally, causing cells to fire. It also allows inhibition at more distant locations to block the spread of excitation, thereby keeping the activity localized in space. Other forms of synaptic architecture have been used to achieve bumps in layered networks of neurons [17, 18]. The conductance-based thalamic model in [17] consists of synaptically interconnected excitatory and inhibitory cell populations, while the single rate equation studied in [18] is derived as a reduction from the thalamic architecture. The synaptic connectivity in these models differs from the Mexican hat structure in that direct connections between excitatory cells are absent. Common to all of these models, however, has been the need for some amount of inhibitory coupling to limit the spread of activity and thereby form the bump. Alternatively, in recent work, Drover and Ermentrout [3] numerically demonstrate the existence of bumps in networks of Type II neurons with purely excitatory synaptic coupling.

In this paper, we show that inhibition is not necessary for bump formation in networks of so-called Type I neurons, which can exhibit oscillations at arbitrarily low frequencies, depending on the input they receive. We study networks composed of two general kinds of Type I neurons, coupled with excitatory synapses into a ring. The first has governing equations that are one-dimensional; a typical example is the "theta" model [8, 4, 11]. The second has governing equations that are two-dimensional, typified by the Morris-Lecar model [14, 16]. The networks that we consider can display quiescent states, where no cells are firing, and active states, with all cells firing. Prior work has shown that starting with the network initially at rest, spatially localized, transient inputs can lead to wave propagation in such networks [6, 15]. We show that appropriate brief inputs to small numbers of cells can generate regions of sustained, localized activity, with only some subset of cells in the network firing and with active cells remaining active indefinitely. Moreover, these networks exhibit multistability of bump solutions of

different sizes.

We use a dynamical systems approach to understand how localized bumps of activity form. We show how geometric phase plane techniques allow us to determine which cells in a network become part of the bump and which stay out. In particular, we find that transient synchrony among the population is important in recruiting cells to the bump, while the eventual desynchrony of these same cells is important both for curtailing the spread of excitation and for sustaining activity of those cells already within the bump. In fact, too much synchrony in the network can cause it to stop oscillating. Ermentrout [4] has shown that for networks of weakly coupled Type I spiking neurons, excitation is desynchronizing. While we don't restrict ourselves to weak coupling, a similar effect is seen in our networks. In fact, it leads directly to one of the main points of this paper: the delay in firing in response to excitation that can occur in Type I neurons can lead to desynchronization, which can in turn decrease the flow of excitatory synaptic current and stop the spread of activity. This yields an an inhibition-free way to achieve spatially localized firing.

Our elucidation of the mechanisms underlying bump formation emphasizes the key role of a geometric feature (the *go curve*), related to the stable manifold of a particular critical point, in selecting whether or not each neuron in a network becomes active. Through simulations and analysis, we find that bump formation is very sensitive to initial conditions and changes in parameters, including amplitude, duration, and width of the transient input that initiates activity. Thus, given a set of parameters, it is difficult to predict whether a bump will form, and if so, what the eventual size of the bump will be. These and other related effects can be clearly understood in terms of the *go curve* and the sensitivity to small perturbations that results from this phase space structure.

It might be postulated that an alternative means to limit the spread of activity in a purely excitatory network, by curtailing synaptic excitation, could come from short-term synaptic depression. It is not at all clear, however, whether synaptic depression that is sufficiently strong to limit activity propagation is compatible with local sustainment of activity. We show that synaptic depression, in general, does promote localized activity in excitatory networks of Type I neurons. Further, depression changes the way that transient inputs influence both bump formation and bump termination, with possible functional implications.

The paper is divided up into several sections. In section 2, we show simulation results from the Morris-Lecar model. This is followed in section 3 by an introduction to the main geometric construct of this paper, the *go curve*, using the theta model. Here we set up the basic framework that is needed to understand bump formation in general networks of Type I cells, and the 1-dimensional nature of the theta model allows for this to be done most clearly. In sections 4 and 5, we go on to analyze the more general two-dimensional Morris-Lecar model, finishing with the inclusion of synaptic depression

in section 5.5. We conclude in section 6 with a Discussion.

2 Numerical Examples: Gradual Recruitment and Bump Formation

We simulated 20 coupled neurons aligned in a ring. The neurons were modeled using the Morris-Lecar equations [14]. In the absence of input, the attractor for each cell was a low-voltage critical point. Each neuron was synaptically connected to its three nearest neighbors on both the left and right sides. Thus neuron 1, for example, was coupled to neurons 2, 3 and 4 on one side and 18, 19 and 20 on the other. Each neuron was also self-coupled. The self-coupling was not strong enough, however, to make an isolated neuron bistable between resting and oscillatory modes. The equations we simulated are

$$\begin{aligned} v_i' &= -I_{Ca} - I_K - I_L - \bar{g}_{syn}[v_i - E_{syn}]\left[c_o s_i + \Sigma_{j=1}^{j=3} c_j[s_{i-j} + s_{i+j}]\right] + I_{ext} \\ w_i' &= [w_\infty(v_i) - w_i]/\tau_w(v_i) \\ s_i' &= \alpha[1 - s_i]H(v_i - v_{thresh}) - \beta s_i, \end{aligned} \tag{1}$$

for $i = 1, \ldots, 20$, where $s_k = s_{k+20}$ for $k < 1$ and $s_k = s_{k-20}$ for $k > 20$. The function $H(v) = 1$ if $v \geq 0$ and is 0 otherwise.

The details of the other functions and parameters involved in equations (1) are given in the Appendix. We point out in particular, however, that with the choice of parameters used, equations (1) generated Type I behavior [16], meaning that each individual cell without synaptic input experiences a saddle-node on an invariant circle, or SNIC, bifurcation as I_{ext} is varied [11, 16]. Further, c_0 is sufficiently small that each cell is not bistable; that is, self-coupling alone is not enough to sustain oscillations if an isolated cell is transiently stimulated.

We performed our simulations using the software XPPAUT [5]. To achieve numerical accuracy, we used the adaptive integrator CVODE with a time step of 0.025 units or smaller. In our simulations, we transiently increased I_{ext} to a small group of cells. We observed the behavior of the entire network for a time period well beyond the initial "shock". We considered a localized activity pattern, or bump, to be stable if the number of cells generating spikes remained invariant for 10000 time units. With a typical spike frequency of about 70-80 spikes per 1000 time units, a simulation of 10000 time units allowed ample opportunity for recruitment of additional cells.

Figure 1 shows what appear to be a stable bump of 7 cells and a stable bump of 13 cells. In both experiments shown, all cells started from rest and then cells 9, 10, and 11, namely the central three cells in a 20 cell network, had I_{ext} raised by 0.2 units for the first 50 time units of the simulation. Under this stimulation, they fired at a relatively high frequency, as can be seen at the top of both panels of Figure 1. After this initial

period, the values of I_{ext} for cells 9-11 were returned to baseline and no subsequent manipulations were performed. Note from the left panel of Figure 1 that cells 7-13 were recruited to fire repetitively, while all other cells remained inactive, forming an activity bump (while cells 5, 6, 14, and 15 do receive some depolarizing input, which causes their v values to rise from baseline as seen in Figure 1, they do not fire.) Further, the fact that the bump consists of 7 cells in this example is a coincidence, rather than a consequence of the fact that each neuron receives synaptic connections from 7 cells (including itself). Indeed, by varying parameters and/or shock conditions, we can obtain bumps of arbitrary size ranging from 3 cells to some parameter-dependent upper bound. In the right panel of Figure 1, recruitment of additional cells continues well beyond the initial shock period, and eventually the network activity appears to stabilize in a 13-cell activity bump. Our numerical simulations lacked sufficient accuracy over the long term to distinguish whether this was truly a stable bump or just a metastable state in which additional cells would fire after a long delay.

For larger values of the coupling strength parameters, all cells in the network eventually become active. Recruitment of cells into the active population occurs at varying rates, depending on these parameters. For a fixed parameter set for which activity spreads, activity does not spread with a constant speed. Instead, delays in the recruitment of each new cell vary widely, as can be seen in Figure 2. We shall comment further on the variability in recruitment delays in Section 5.4.

3 Theta neuron model

For analytical purposes, we first describe a one-dimensional Type I model known as the theta neuron. In Figure 3, we show a simulation of a ring of 20 theta neurons which exhibits a bump of 8 cells. The figure was produced by transiently shocking the 4 central cells as shown in the figure. Using the theta model, we shall easily be able to describe an important geometric construct known as the *go curve*, which we shall use throughout the text. The dynamics of a theta neuron in the absence of synaptic input are governed by the equation

$$\theta' = 1 - \cos\theta + b(1 + \cos\theta). \tag{2}$$

The derivative in (2) is with respect to the variable t. The neuron is said to "fire" when θ increases through the value $(2n+1)\pi$ for any integer n. For $b < 0$, there exist two critical points of (2), given by $\theta_S = -\cos^{-1}(1+b)/(1-b)$ and $\theta_U = \cos^{-1}(1+b)/(1-b)$. The first is stable, while the second is unstable. The phase circle for this neuron is shown in Figure 4.

Now consider a ring of N neurons. Each neuron as before is connected to its three nearest neighbors on either side. In particular neuron 1 gets input from neurons 2, 3 and 4 as well as $N-2$, $N-1$ and N. The total synaptic input to the ith neuron is

given by $g_{i_{syn}} = \bar{g}_{syn}\left[c_o s_i + \Sigma_{j=1}^{j=3} c_j[s_{i-j} + s_{i+j}]\right]$, with adjustments at the boundaries as in (1), where $c_1 > c_2 > c_3 \geq 0$ are distance dependent coupling strengths and $c_0 \geq 0$ is the strength of self-coupling. Note that the nonnegativity of the coupling constants corresponds to excitatory coupling. The equations for each neuron are now

$$\begin{aligned} \theta_i' &= 1 - \cos\theta_i + (1+\cos\theta_i)(b + g_{i_{syn}}) \\ g_{i_{syn}}' &= -\beta g_{i_{syn}} \\ s_j' &= -\beta s_j, \quad j = i-3, \ldots i+3. \end{aligned} \tag{3}$$

The synaptic variable s_j is reset to one whenever the jth neuron fires. This has the effect of resetting $g_{i_{syn}}$ to a higher value whenever any of the neurons $i-3$ to $i+3$ fire. One effect of synaptic coupling is to change the values of θ_S and θ_U. When $g_{i_{syn}} < -b$, there continue to exist two critical points given by

$$\begin{aligned} \theta_S(g_{i_{syn}}) &= -\cos^{-1}\tfrac{1+b+g_{i_{syn}}}{1-b-g_{i_{syn}}} \\ \theta_U(g_{i_{syn}}) &= \cos^{-1}\tfrac{1+b+g_{i_{syn}}}{1-b-g_{i_{syn}}}. \end{aligned} \tag{4}$$

When $g_{i_{syn}} = -b$, these two critical points merge at a saddle-node bifurcation and they disappear for $g_{i_{syn}} > -b$. This can very easily be depicted in a $\theta_i - g_{i_{syn}}$ phase plane as shown in Figure 5. The parabolic shaped curve $\mathcal{P}$ represents the critical points (4) as functions of $g_{i_{syn}}$. The vector field of (3) points down on $\mathcal{P}$ since $\theta_i' = 0$ and $g_{i_{syn}}' < 0$ there. Notice that this curve intersects the horizontal axis at $(\theta_S, 0)$ and $(\theta_U, 0)$. The unstable critical point $(\theta_U, 0)$ is a critical point of the first two equations of (3). In fact, it is a saddle point with a one-dimensional unstable manifold, which lies along the horizontal axis, and a one-dimensional stable manifold. One branch of this stable manifold lies in the positive $g_{i_{syn}}$ part of the $\theta_i - g_{i_{syn}}$ phase plane as shown in Figure 5.

This one-dimensional stable manifold traces out a curve which we call the *go curve*. It is the unique trajectory which approaches $(\theta_U, 0)$ in the positive $g_{i_{syn}}$ part of the $\theta_i - g_{i_{syn}}$ phase plane. It is invariant under the flow of (3), meaning that trajectories cannot cross over it. We call it the *go curve* because it separates the $\theta_i - g_{i_{syn}}$ phase plane into regions of initial conditions which are either attracted to the asymptotically stable critical point at $(\theta_S, 0)$ (below the *go curve*) or are eventually pushed off this phase plane through the right vertical boundary $\theta = 1.75$ (above the *go curve*); see Figure 5. Note, however, that the *go curve* is temporarily irrelevant whenever one or more of the s_i are reset to the value one. Whenever any s_i is reset to 1, $g_{i_{syn}}$ is also reset to a higher value. This causes the trajectory of neuron i to be shifted vertically in the $\theta_i - g_{i_{syn}}$ phase plane by an amount corresponding to the synaptic input. This may cause the trajectory of neuron i to be reset above the *go curve*. If this occurs, then neuron i will fire. If the neuron i is not reset above the *go curve* for any synaptic input,

then it will not fire. Figure 6 shows an example of a cell which receives several synaptic inputs before it is eventually reset above *go curve*, after which time it fires.

4 General two-dimensional model

4.1 Intrinsic properties

We now consider more general equations which encompass the Morris-Lecar equations and develop a theory that explains the numerical results shown in section 2. For this more general model, the dynamics of each cell are described by two first-order equations, generically of the form

$$\begin{aligned} v' &= f(v,w) + I_{ext} \\ w' &= [w_\infty(v) - w]/\tau_w(v). \end{aligned} \tag{5}$$

For simplicity, the time constant $\tau_w(v)$ is defined to be τ_L when $v < v_{thresh}$ and τ_R otherwise. The v-nullcline, given by the set $\{(v,w) : f(v,w) + I_{ext} = 0\}$, is assumed to be a cubic-shaped curve. It has two local extrema, or knees, namely a left knee (v_{LK}, w_{LK}) and a right knee (v_{RK}, w_{RK}) with $v_{LK} < v_{RK}$ and $w_{LK} < w_{RK}$. The w-nullcline, given by $\{(v,w) : w_\infty(v) - w = 0\}$, is assumed to be a sigmoidal shaped curve. By rescaling f if necessary (e.g. adding 0.075 to f for the Morris-Lecar system described in the Appendix), we can assume that when $I_{ext} = 0$, these two nullclines intersect at three points labeled (v_l, w_l), (v_m, w_m) and (v_u, w_u). The point (v_l, w_l) lies on the left branch of the cubic, while the other two points lie on its middle branch. These intersections represent critical or equilibrium points of the system; only (v_l, w_l) is stable. See Figure 7.

The term I_{ext} represents an external applied current. Increasing I_{ext} raises the cubic-shaped v-nullcline in the $v - w$ phase plane. The position of the critical points of the system (5) change as I_{ext} is changed. As I_{ext} is smoothly increased, the critical point on the left branch and the closer one along the middle branch meet at the local minimum of the v-nullcline, forming a saddle-node on an invariant circle (SNIC) bifurcation. This bifurcation gives rise to a periodic solution of the set of equations (5). This periodic orbit encircles the one remaining critical point along the middle branch of the cubic-shaped curve and represents an action potential of the neuron; see Figure 7. The action potential is characterized by two parts: its active phase and its silent phase. The active phase is defined to be any portion of the cell's trajectory for which $v > v_{thresh}$. For the sake of simplicity, we shall assume that any active phase of any cell has time duration t_{ap}. The silent phase is the portion of the trajectory for which $v < v_{thresh}$. The majority of this time is spent near the left branch of the v-nullcline. The larger τ_L is, the closer the trajectory lies to this branch.

4.2 Synaptic coupling between cells

We consider a network of N neurons aligned in a ring. Without loss of generality, take $I_{ext} = 0$ for each cell. As before, the firing of neuron i leads to excitatory synaptic inputs through a variable s_i. The dynamics are somewhat different than in the theta neuron model case, since for the current two-dimensional model, each neuron spends a non-zero amount of time in the active state. We assume the excitation to be fast rising, but slowly decaying, similar to an NMDA-mediated synapse. This is modeled by the variable s_i, which obeys the equation

$$s_i' = \alpha[1 - s_i]H(v_i - v_{thresh}) - \beta s_i. \tag{6}$$

We shall assume for the analysis that the rise rate of the synapse is arbitrarily large, $\alpha \to \infty$. This implies that as soon as $v_i \geq v_{thresh}$, s_i is set to the value 1, as in the theta neuron model. But now, s_i remains at this value for the active duration t_{ap}, until $v_i < v_{thresh}$, after which $s_i' = -\beta s_i$, where β is the decay rate of the synapse. As before, in our ring of N neurons, we assume that each neuron is coupled to its three neighboring neurons to either side of itself. Each neuron is also self-coupled. The equations of interest are

$$\begin{array}{rcl} v_i' & = & f(v_i, w_i) - \bar{g}_{syn}[v_i - E_{syn}]\left[c_0 s_i + \Sigma_{j=1}^{j=3} c_j s_{i-j} + s_{i+j}]\right] \\ w_i' & = & [w_\infty(v_i) - w_i]/\tau_w(v_i) \end{array} \tag{7}$$

and

$$s_i' = -\beta s_i \quad \text{if } v_i < v_{thresh} \tag{8}$$

OR

$$s_i = 1 \quad \text{if } v_i \geq v_{thresh}. \tag{9}$$

Notice that at any moment in time when cell i and all of its six neighbors are below v_{thresh}, the equations governing cell i can be written more compactly. Indeed, if, as before, we let $g_{i_{syn}} = \bar{g}_{syn}\left[c_0 s_i + \Sigma_{j=1}^{j=3} c_{[} s_{i-j} + s_{i+j}]\right]$, then

$$\begin{array}{rcl} v_i' & = & f(v_i, w_i) - g_{i_{syn}}[v_i - E_{syn}] \\ w_i' & = & [w_\infty(v_i) - w_i]/\tau_w(v_i) \\ g_{i_{syn}}' & = & -\beta g_{i_{syn}}. \end{array} \tag{10}$$

Let $F(v_i, w_i, g_{i_{syn}})$ denote the right-hand side of the first equation of (10).

The effect of the excitatory synapse on the v-nullcline of an individual cell is to raise it in the $v - w$ phase plane. If $g_{i_{syn}}$ is increased a small amount from 0, then the critical point on the left branch of the ensuing cubic will remain. If $g_{i_{syn}}$ is made large enough, then the critical point on the left branch will be lost through a SNIC bifurcation, and oscillations will ensue. This is analogous to the effect of raising I_{ext} discussed in Section 4.1, except that the effect of excitatory synapses on cell v_i depends on v_i, through the term $(v_i - E_{syn})$ in equation (10).

5 Geometry of Bumps

To determine how stable bumps can arise purely through excitatory coupling, we primarily need to understand two things: one, how do cells either get recruited or fail to get recruited into a bump, and two, how do the recruited cells sustain their oscillations. Once these aspects are clear, we will show how bumps are formed and discuss characteristics of the bumps.

5.1 The *go curve* when $w_i' = 0$

We shall begin by considering a simplified scenario in which we assume that for a certain part of the cell's trajectory its w value is fixed (i.e., $w' = 0$). This case will be very similar to that which occurred for the theta neuron model. We will use the concept of the *go curve* to illustrate the idea of recruitment of cells into a bump. We will then go on to generalize these geometric constructs to the full $w' \neq 0$ flow, where we discuss both recruitment into a bump and sustainment of oscillations.

5.1.1 The $v_i - g_{i_{syn}}$ phase plane

Conceptually, the $v_i - g_{i_{syn}}$ phase plane is similar to that of the $\theta_i - g_{i_{syn}}$ phase plane of section 3, Figure 5. There are some important differences, however, due to fact that the intrinsic equations of each oscillator are now two-dimensional.

Consider cell i to be at rest at the critical point $(v_l, w_l, 0)$, which is the stable critical point of equations (10). A straightforward way to understand the effect of excitation on a cell i is to consider a $v_i - g_{i_{syn}}$ phase plane in a cross section of fixed w_i, assuming $w_i' = 0$. The upper part of Figure 8 gives a schematic representation of how the position of the cubic v-nullcline changes in $v - w$ space as $g_{i_{syn}}$ is increased. The dashed horizontal line along the slice $w = w_l$ has been selected here for illustration. The nullcline associated with $g_{i_{syn}} = 0$ intersects this slice at exactly two points, while the nullcline associated with $g_{i_{syn}} = g_2$ intersects this slice at exactly one point. Any nullcline associated with a $g_{i_{syn}} = g_1$, where $g_1 \in (0, g_2)$, intersects the slice in two points as pictured. If $g_{i_{syn}} > g_2$, then there are no intersections. In the lower part of Figure 8, the points of intersection for $g_{i_{syn}} \in [0, g_2]$ are pictured in the parabola-like curve labeled $\mathcal{P}$ in the $v_i - g_{i_{syn}}$ phase plane. The vector field of (10) points down on $\mathcal{P}$ since $v_i' = 0$ there. This is qualitatively the same as for the theta neuron model. Note that in Figure 5, the parabolic curve represents the fixed points of (3) for different values of $g_{i_{syn}}$. In the present case, the parabolic curve represents the fixed points of the first equation of (10) for different values of $g_{i_{syn}}$ when $w_i = w_l$ is a fixed quantity. Note also that $\mathcal{P}$ is asymmetric, since the v-nullclines are not symmetric about their minima.

When we visualize the $v_i - g_{i_{syn}}$ phase plane, we naturally restrict to $g_{i_{syn}} \geq 0$. For convenience, we bound the v_i-values that we consider in the $v_i - g_{i_{syn}}$ phase plane.

Specific choices of boundary values of v_i are not important, however, as long as we consider a sufficiently large neighborhood of $\mathcal{P}$. For convenience, we will specify the right boundary as $v_i = v_{thresh}$, and we will denote the left boundary as $v_i = v_{min}$. The left point of intersection of $\mathcal{P}$ with the segment $\{g_{i_{syn}} = 0\}$ in the lower part of Figure 8 is $(v_l, 0)$, which is the projection to the $v_i - g_{i_{syn}}$ plane of the critical point $(v_l, w_l, 0)$ of the full system. The other intersection point is at $(v_{c_m}, 0)$, where v_{c_m} is obtained as the solution of $f(v_{c_m}, w_l) = 0$ and (v_{c_m}, w_l) lies along the middle branch of the cubic v-nullcline in $v - w$ space for $g_{i_{syn}} = 0$.

In the $v_i - g_{i_{syn}}$ phase plane, holding $w_i = w_l$ fixed, we consider the flow given by the v_i and $g_{i_{syn}}$-equations from (10). Under this flow, the point $(v_l, 0)$ is asymptotically stable, while the point $(v_{c_m}, 0)$ is an unstable saddle point. Its unstable manifold lies along the horizontal v_i axis, and one branch of its stable manifold lies on the positive $g_{i_{syn}}$ part of the $v_i - g_{i_{syn}}$ phase plane as shown in Figure 9. As in Section 3, this one-dimensional stable manifold traces out a curve which we label the *go curve*. It is the unique trajectory which approaches $(v_{c_m}, 0)$ in the positive $g_{i_{syn}}$ part of the $v_i - g_{i_{syn}}$ phase plane. It is invariant under the flow of (10) with $w_i' = 0$, meaning that trajectories cannot cross over it; see Figure 9. Note, as before, that the *go curve* is temporarily irrelevant when one or more of the s_i satisfy equation (9) instead of equation (8). During such periods, trajectories may switch sides of the *go curve*. This is precisely how a synaptic input can cause a cell to fire (see below).

The intersection of the sigmoidal w-nullcline and the left branch of the cubic v-nullcline for system (10) changes as a function of $g_{i_{syn}}$. Note that the maximal amount of excitation any cell can receive is $g_{max} = \bar{g}_{syn}[c_o + 2c_1 + 2c_2 + 2c_3]$. Let w_{max} be the w-value of the minimum of the cubic associated with g_{max}, i.e. it is the minimum of the two solutions to $F(v, w, g_{max}) = 0$ and $\partial F(v, w, g_{max})/\partial v = 0$. Recall that the $v_i - g_{i_{syn}}$ phase plane above was defined in the horizontal slice $w_i = w_l$. We may define similar $v_i - g_{i_{syn}}$ phase planes for different fixed w_i values whenever $w_i \in [w_l, w_{max}]$, making the assumption $w_l < w_{max}$. The v_i-axis would correspond to an absence of synaptic input for that fixed w_i value being considered. For example, if $w_i = \bar{w} \in (w_l, w_{max})$, then the parabola $\mathcal{P}$ intersects this axis at two points which satisfy $F(v, \bar{w}, 0) = 0$. The left and right boundaries of the $v_i - g_{i_{syn}}$ phase plane remain as previously, independent of the choice of w_i. We will exploit this to look at the $(v, g_{i_{syn}})$ phase plane for various w values when we allow w to vary below.

5.1.2 Recruitment versus non-recruitment: $w_i' = 0$

We now consider a single cell i that can potentially receive synaptic input from its neighboring cells. Let cell i start at $t = 0$ at rest at the stable critical point $(v_l, 0)$ in the $v_i - g_{i_{syn}}$ phase plane for the slice $w = w_l$. The effect of excitation is to instantaneously change its location in the $v_i - g_{i_{syn}}$ phase plane, moving it vertically by an amount

determined by the synaptic input size. For the sake of argument, suppose cell i receives a single dose of excitation at $t = 0$ from cell $i-1$. Then cell i is reset at $t = 0^+$ to the position $(v_l, \bar{g}_{syn}c_1)$. For the length of time of an action potential of the presynaptic cell, t_{ap}, $g_{i_{syn}}$ does not change, but v_i does. Starting from $t = t_{ap}^+$, the evolution of $g_{i_{syn}}$ is given by equation (10), such that the *go curve* becomes relevant. If $(v_i(t_{ap}), \bar{g}_{syn}c_1)$ lies below the *go curve*, then with no further synaptic input, cell i will return to rest at $(v_l, 0)$ and will not be recruited. Alternatively, if the new position lies above the *go curve*, then even with no further synaptic input, cell i will escape the $v_i - g_{i_{syn}}$ phase plane through the boundary $v = v_{thresh}$ and fire an action potential. In this case, cell i will have been recruited into the bump pattern. Both of these cases are illustrated by the trajectories shown in Figure 9. Note that if cell i does receive additional input after crossing above the *go curve*, this cannot prevent cell i from firing, since $\bar{g}_{syn}$ and all c_i are positive and $v_i' > 0$ above the *go curve*.

When cell i receives more than one synaptic input from its neighboring cells, the rule for recruitment or non-recruitment remains the same. Namely, cell i will be recruited into the bump pattern if and only if the summed synaptic input $g_{i_{syn}}$ allows cell i to be reset such that it lies above the *go curve* when $g_{i_{syn}}$ resumes following the dynamics of (10). Note that all recruitment is one-sided. Only the synaptic inputs from cells $i-1$, $i-2$ and $i-3$ are relevant, since cells $i+1$, $i+2$ and $i+3$ have yet to be recruited into the bump and thus $s_{i+1} = s_{i+2} = s_{i+3} = 0$. The timing of synaptic inputs to cell i is an important factor in determining if it will be recruited. Suppose that cell i receives synchronized synaptic input $g_{i_{syn}} = \bar{g}_{syn}[c_1 + c_2 + c_3]$ from its three left neighbors. The strengths $\bar{g}_{syn}$, c_1, c_2 and c_3 are chosen so that this amount of synchronized input resets cell i above the *go curve* after time t_{ap}. Thus cell i will be recruited; see Figure 10 position A. If, however, the input from the neighbors is desynchronized, say cell $i-2$ fires at $t = 0$, but $i-3$ and $i-1$ fire at time $t = t_1 > 0$, then cell i may fail to fire. The input at $t = 0$ will now be $g_{i_{syn}} = \bar{g}_{syn}c_2$, and let's suppose for the sake of argument that this resets cell i below the *go curve*; see position B of Figure 10. Now cell i evolves in the $v_i - g_{i_{syn}}$ phase plane with $g_{i_{syn}}$ decreasing with rate β. Note that trajectories move away from the *go curve* as t evolves, since the *go curve* is the stable manifold of the saddle point $(v_{c_m}, 0)$. The next synaptic input occurs at $t = t_1$ and resets $g_{i_{syn}}$ to $\bar{g}_{syn}[c_1 + c_2\exp(-\beta t_1) + c_3]$. Thus if the time t_1 is too large, then the reset level may again fall below the *go curve*, again failing to recruit cell i; an example of this is seen in Figure 10 when the trajectory at position C is reset to position D. However, if t_1 is small, then the reset level may be above the *go curve*, causing recruitment; an example of this occurs in Figure 10 when the trajectory at position E is reset to position F.

In short, tightly synchronized synaptic input promotes recruitment. This is not surprising, but a key point is that the timing of inputs affects the amount of input required for recruitment to occur. This dependence can be seen directly by calculating the reset level of $g_{i_{syn}}$ and checking its relationship to the *go curve*. It can also be inferred

from the fact that trajectories move away from the *go curve*. Thus, when inputs to cell i are more spaced out in time, they must be larger to push cell i above the *go curve*.

5.2 The *go surface* when $w_i' \neq 0$

We now turn our attention to the more realistic case in which we do not assume that $w_i' = 0$ in the $v_i - g_{i_{syn}}$ phase plane. As a consequence, instead of having a one-dimensional *go curve*, we must now construct a two-dimensional *go surface*. Beyond this change, the idea behind recruitment remains as in the prior sections; cell i is recruited if and only if a synaptic input resets its position to lie on the appropriate side of the *go surface*. We will show how this can be studied in a three-dimensional $v_i - w_i - g_{i_{syn}}$ phase space and also show how the flow can be projected down to an appropriate two-dimensional $v_i - g_{i_{syn}}$ phase plane.

5.2.1 The $v_i - w_i - g_{i_{syn}}$ phase portrait

The point $(v_m, w_m, 0)$ is a critical point for the set of equations (10). By linearizing, it is easy to see that this point has a two-dimensional stable manifold W^s and a one-dimensional unstable manifold W^u. The two-dimensional stable manifold, as shown in Figure 11, divides the phase space defined by $M = \{(v_i, w_i, g_{i_{syn}}) : w_i \geq 0, g_{i_{syn}} \geq 0, v_{min} \leq v_i \leq v_{thresh}\}$ into two parts; in Figure 11, one part lies to the left of W^s and the other lies to the right of W^s. Moreover, W^s is invariant under the flow of (10), implying that trajectories cannot cross it in $v_i - w_i - g_{i_{syn}}$ phase space. As before, trajectories can be reset to the opposite side by synaptic inputs, however, since instantaneous increases in $g_{i_{syn}}$ are not governed by equation (10). Therefore under appropriate conditions, W^s separates trajectories in phase space which are either attracted to the asymptotically stable critical point $(v_l, w_l, 0)$, and thus are blocked from leaving M, from those which eventually leave M through the boundary $v_i = v_{thresh}$. We will thus call W^s a *go surface*. The two-dimensional *go surface* W^s is a natural generalization of the one-dimensional *go curve* that we had considered in prior sections. It is important to note that since the synaptic input is excitatory, increases in s can reset trajectories from the blocked side of the *go surface* to the side of the *go surface* from which they can escape, but not vice versa.

5.2.2 Recruitment versus non-recruitment: $w_i' \neq 0$

Suppose cell i is at rest at $(v_l, w_l, 0)$ at $t = 0$ and receives synaptic input from cell $i-1$ at this time. Its position is then immediately reset to $(v_l, w_l, c_1\bar{g}_{syn})$. At $t = t_{ap}$, cell $i-1$ falls below v_{thresh} and its excitation to cell i begins to decay. If the position $(v_i(t_{ap}), w_i(t_{ap}), c_1\bar{g}_{syn})$ lies to the left of the *go surface* W^s, then cell i will not be recruited into the activity pattern. If it lies to the right of W^s, then it will be recruited.

By projecting out w_i, it is possible to decide whether a cell is recruited or not by studying an appropriate two-dimensional $v_i - g_{i_{syn}}$ phase plane. In particular, if cell i received a synaptic input at $t = 0$, then we consider the intersection of W^s with the plane $w_i = w_i(t_{ap})$. This intersection of two two-dimensional manifolds creates a one-dimensional *go curve*. The *go curve* is then projected down onto a $v_i - g_{i_{syn}}$ phase plane. Note that unlike the *go curve* in the case when $w_i' = 0$, the *go curve* here, in general, is not invariant under the flow of (10). As a result, trajectories can also cross over the shown *go curve*. The reason for the the lack of invariance is that on the projected $v_i - g_{i_{syn}}$ phase plane, w_i changes since $w_i' \neq 0$. The *go curve* shown is for a specific value of $w_i = w_i(t_{ap})$ and only separates recruited from non-recruited trajectories in the $v_i - g_{i_{syn}}$ phase plane *at the single moment in time* $t = t_{ap}$. Thus cell i is recruited if it lies above this *go curve* at $t = t_{ap}$. For any $t > t_{ap}$, a new *go curve* could be obtained as the intersection of W^s with $w_i = w_i(t)$. However, because the *go surface* W^s is invariant under the flow of (10), if cell i lies to the left (right) of W^s at $t = t_{ap}^+$, then it remains to the left (right) for all $t > t_{ap}$ in the absence of new inputs, although subsequent inputs may push cells from the left side of W^s across to the right side of W^s. Projected down to the $v_i - g_{i_{syn}}$ phase plane, the invariance of W^s implies that once a trajectory is reset to lie above the relevant *go curve*, the trajectory will remain above every relevant *go curve* until it reaches $v = v_{thresh}$, and if a trajectory is below the relevant *go curve*, then it will remain below every relevant *go curve* until it receives additional input.

When cell i receives more than one synaptic input, there are now several *go curves* to consider. For the sake of argument, suppose cell $i-1$ and $i-2$ fire at times t_1 and t_2, respectively, where $t_1 < t_2$. We construct two different *go curves* by finding the intersection of W^s with $w_i(t_1 + t_{ap})$ and its intersection with $w_i(t_2 + t_{ap})$. Each *go curve* serves to separate the $v_i - g_{i_{syn}}$ phase plane at exactly one moment in time, namely $t = t_1 + t_{ap}$ or $t = t_2 + t_{ap}$ respectively. At either of those times, if the trajectory lies above the relevant *go curve*, then cell i will be recruited. Figure 12 shows results from a simulation of 20 cells aligned in a one-dimensional chain (non-periodic boundary conditions) in which cells 1-3 are transiently shocked and a stable 6-bump develops. The trajectory of cell 6, which is synaptically connected to its six neighbors and which is eventually recruited into the bump, is shown. At $t = 0$, cell 6 is at rest near the location $(-0.305, 0)$. Its trajectory over time is shown as the bold solid curve. Notice that it receives several synaptic inputs of different sizes during the time shown (ten to be precise), each characterized by a rapid increase in the $g_{i_{syn}}$ value. A *go curve* associated with each input is constructed as described before. In Figure 12, we show the *go curves* associated with the 8th, 9th, and 10th inputs which are constructed to occur at $t_8 + t_{ap}$, $t_9 + t_{ap}$, and $t_{10} + t_{ap}$, respectively. Notice that the position of the trajectory at $(v_i(t_8 + t_{ap}), g_{i_{syn}}(t_8 + t_{ap}))$ lies below the *go curve* associated with the 8th input (labeled "first" in the blown up figure on the right). Thus, had there been no further synaptic input, cell 6 would not have been recruited. However, note that at

$t = t_9$, and also at $t = t_9 + t_{ap}$, the trajectory lies above the 9th *go curve* ("second"). Thus, we see that the 9th input causes the cell to be recruited. Of course, the trajectory also lies above the corresponding dash-dotted *go curve* at $t = t_{10} + t_{ap}$, as it will for all relevant *go curves* for all subsequent time until it escapes the $v_i - g_{i_{syn}}$ phase plane through the right boundary. Indeed, in Figure 13, we see that if the 10th synaptic input is artificially blocked, then cell 6 is still recruited. It is interesting to note that the input that actually pushed the cell over the *go curve* was relatively very small. This illustrates how cooperativity of inputs can lead to recruitment of cells and how exceedingly small inputs can have a large effect on a cell's activity pattern.

5.2.3 The role of the synaptic decay rate in recruitment

Consider again the case $w_i' = 0$. For fixed w, linearization of the equations

$$\begin{aligned} v' &= f(v,w) - g_{i_{syn}}(v - E_{syn}) \\ g_{i_{syn}}' &= -\beta g_{i_{syn}}, \end{aligned}$$

about the saddle point $(v_{c_m}, 0)$ yields the matrix

$$\begin{pmatrix} \frac{\partial f}{\partial v} & -(v_{c_m} - E_{syn}) \\ 0 & -\beta \end{pmatrix}$$

where $\partial f/\partial v > 0$. The eigenvector v_s corresponding to the stable eigenvalue $-\beta$ is a multiple of $(v_{c_m} - E_{syn}, \partial f/\partial v + \beta)$.

As the synaptic decay rate β becomes larger, the positive term $\partial f/\partial v + \beta$ becomes larger. Since $v_{c_m} - E_{syn} < 0$, corresponding to excitatory input, the slope of the eigenvector v_s becomes more negative, i.e. the *go curve* becomes more vertical. Thus, given $\beta_1 < \beta_2$, the *go curve* associated with β_1 lies below that associated with β_2. Therefore greater synaptic excitation is needed to achieve recruitment for larger β.

A similar calculation gives the same result when $w_i' \neq 0$. Thus, slow synaptic decay promotes recruitment of cells into the active group. In the next subsection, we shall see that there is a second, more direct way in which slow synaptic decay contributes to sustainment of activity.

5.2.4 Sustainment

We now discuss how a cell remains in the bump pattern once it has been recruited. The criterion for sustainment of activity is similar to that for recruitment. Suppose that cell i has fired at $t = 0$ and has returned to the silent phase at some later time. Next, suppose that at $t = t_1 > 0$, $w_i(t_1) \in [w_l, w_{max}]$ and cell i receives synaptic input because one of its neighboring cells just fired. At the end of the neighbor's action potential,

we consider the $v_i - g_{i_{syn}}$ phase plane in the horizontal slice $w = w_i(t_1 + t_{ap})$ and ask whether or not cell i has been reset above the *go curve* of that phase plane or not. If it has, it will fire again and its oscillation will be sustained for at least one more cycle.

Clearly, self-coupling boosts the synaptic input to cells that have already fired, relative to those that have not, contributing significantly to sustainment. Two additional features also promote sustainment of oscillations beyond what has already been discussed for recruitment, namely the desynchronized arrival, and subsequent slow decay, of the excitatory synaptic input. We discussed above how slow synaptic decay affects the slope of the *go curve*, and hence the recruitment of cells. For activity to be sustained, the decay rate β of each synapse must also be chosen small enough relative to the inverse of the time constant τ_L so that once cell i fires, it will have enough residual excitation left from the prior cycle to be reset above the *go curve* of the relevant $v_i - g_{i_{syn}}$ phase plane when it again receives synaptic input. The role of this residual input is simply to keep cells closer to a relevant *go curve* than without the input. Thus, additional synaptic inputs may be able to fire cells due to the residual excitation in situations where the additional inputs alone could not fire the cells. In particular, we note that residual excitation is not strong enough to allow a cell to fire a second time in the absence of additional synaptic input.

It is also important for sustainment of activity that all cells in the bump are not actually synchronized, as noted in other studies [9, 13, 17]. Suppose that the stable critical point on the left branch of the cubic v-nullcline persists for any relevant value of $g_{i_{syn}}$. Thus, if all cells fire together, then after their action potentials end, they will not be able to fire again. Since they are synchronized, there cannot be any other cells available to provide excitation at a later time. Thus, some amount of desynchronization within the bump is necessary to sustain oscillations. In fact, in our network, a perfectly synchronous bump solution does not exist.

5.3 Bump formation

Bump formation requires three elements: recruitment, cessation of recruitment, and sustainment. The work of the previous subsections highlights two competing effects of synchrony (or alternatively desynchrony). Synchronization of synaptic inputs promotes recruitment, but too much synchrony opposes sustainment. Thus, in order to have stable, localized activity, there must exist a balance of these two effects. Further, to create bumps from localized transient inputs, the work of the above subsections suggests that initial tight synchronization of cells, followed by their gradual desynchronization, would be helpful. We now turn to why synchrony breaks down and recruitment ends in our network.

In the left simulation shown in Figure 1, we raised I_{ext} to cells 9, 10 and 11 for a duration of 50 time units, thereby instigating rhythmic activity and allowing these

cells to oscillate at high frequency. These oscillations are tightly synchronized because the cells all converge to the same zero-input rest state, namely $(v_l, w_l, 0)$, before being shocked, and any desynchronizing effects from synaptic coupling are weak relative to the common input I_{ext} during the shock.

The synchrony of this core group of cells caused neighboring cells (7,8, 12 and 13) to be recruited into the bump pattern; see Figure 1. The initial close synchrony of cells 9, 10 and 11 is fairly quickly destroyed, however, once the shock ends. In fact, there is no synchronous periodic solution for the set of parameters that we have chosen. Thus, the cells are able to continue oscillating precisely because they desynchronize, as discussed in Section 5.2.4 on sustainment,

The reason the cells lose synchrony has to to do with the manner in which they are reset to the opposite side of the *go surface*. Recall that the *go surface* is the stable manifold W^s of the point $(v_m, w_m, 0)$. Any trajectory which lies on W^s will remain there unless an additional input resets it off of W^s. Moreover, due to its attractive properties, any point that lies arbitrarily close but to the right of W^s can take an arbitrarily long time to leave a neighborhood of W^s and cross v_{thresh}. This fact induces a sensitive dependence on initial conditions. Namely, cells that start close together in phase space may cross v_{thresh} at dramatically different times. This, in turn, may mean that their trajectories are very far apart in phase space at later times. This has the effect of desynchronizing cells.

The loss of synchrony is not only important in maintaining oscillations within the network, it is also crucial to why excitation does not spread throughout the entire cell assembly. We have chosen the parameters $\bar{g}_{syn}$, c_1, c_2 and c_3 small enough so that if cell i is near rest and receives synaptic input from only one of its neighbors, then it cannot be recruited into the bump. To see this, note that the largest single input a cell can receive has size $\bar{g}_{syn}c_1 = .022$ in most simulations, and see for example Figure 9, which shows that inputs need to have magnitude greater than .04 to push a cell over the *go curve* from near rest. The case with $w' \neq 0$ gives a similar result. This parameter setting implies that even if cell i is recruited into the bump, there is no guarantee that cell $i+1$ will also be recruited. As a bump progresses, and subsequent cells are recruited, the cells that are firing gradually desynchronize. This means that the inputs to potential recruits outside of the bump are spreading out in time, and when subsequent cells are recruited by passing through the *go surface*, they may end up closer to the *go surface* than their predecessors had been when they were recruited. As a result, new recruits may experience more delay between crossing the *go surface* and actually firing, and this further desynchronizes the population of active cells. Eventually, the inputs to non-firing cells become sufficiently desynchronized that they fail to recruit any additional cells.

5.4 Implications of the go surface

The bumps that we have discussed are non-robust in the sense that small changes in parameters can change bump size. This follows from the realization that cells that join the bump and cells that do not are differentiated by their relations to the *go surface*. Indeed, the cells just outside the bump come very close to the *go surface* due to the inputs that they receive (see Figure 14). Small increases in these inputs could push them across.

We emphasize that whether an input or combination of inputs succeeds in recruiting a cell cannot be predicted simply from its magnitude. Figure 15 shows $g_{i_{syn}}$ versus time from the same trajectories shown in Figure 14. ¿From Figure 14, note that the input that pushes the recruited cell over the *go curve* raises $g_{i_{syn}}$ for that cell from about .0125 to about .027. This is the first part of the second large peak in the dashed curve in Figure 15, which appears to be tangent to the dotted line at $g_{i_{syn}} \approx .027$. The synaptic conductance $g_{i_{syn}}$ for the non-recruited cell exceeds this value several times even in the short simulation shown in these figures, yet it fails to cross the go surface.

A more functionally advantageous consequence of this sensitivity to synaptic coupling strengths is that it is possible to form bumps of a range of sizes, for fixed parameter values, by shocking a small group of cells with transient inputs of varying durations. Suppose parameters are set so that each cell requires fairly synchronized firing of all of the cells that send it synaptic input in order to initially fire. During the shock period, the transient external inputs cause the cells that receive them to fire at frequencies in excess of the firing rates that they would normally exhibit. This leads to strong synaptic inputs to their neighbors, recruiting them easily into the bump and causing them to fire faster than otherwise expected. Thus, the influence of the shock becomes cyclical: cells fire faster, generating stronger synaptic outputs, which causes subsequent cells to fire faster, and so on. The net effect is to promote the spread of activity throughout the network.

Once the shock is turned off, the cells within the bump immediately begin to slow down and desynchronize [4]. For large ranges of parameter values, this causes bump propagation to end once the shock is removed. The cells already in the bump, however, receive self-coupling, in addition to the synaptic inputs from other cells. This is enough to allow their firing to persist, in light of the effects of desynchronization, mediated by the *go surface*, discussed in earlier sections. Thus, a range of bump sizes can be achieved by variation of shock duration.

Depending on parameters, however, there may be an upper limit on how far activity will spread, even when the shock is on. Each newly recruited cell is recruited with a smaller synaptic input than the cell before it. This means that the input that resets the new recruit above the *go surface* leaves it closer to the *go surface*, causing a longer delay before firing, as discussed above. This causes activity away from the shocked region to

become progressively more desynchronized. Eventually, the inputs to some cells outside the bump may be too desynchronized to recruit them. In fact, for the parameters used in Figure 1, a bump of 9 cells forms if the shock of $I_{ext} = 0.2$ is maintained for any duration of time greater than about 100 time units.

Besides the generation of different bump sizes from different shock protocols, an additional implication of the *go surface* is that even when activity spreads throughout an entire network of cells, there can be quite variable delays between the recruitment times of adjacent cells, as seen in Figure 2. Suppose that the coupling strengths are sufficiently strong such that if cell i at $(v_l, w_l, 0)$ receives precisely synchronized inputs from cells $i-3, i-2$, and $i-1$, then it will cross the *go surface* and eventually fire. The complex fluctuations of relative firing times of cells in the bump, which derive from the positions of the cells relative to the *go surface*, can allow sufficient synchrony to transiently develop to recruit a cell from the outside edge of the bump, sometimes with a long delay since the previous recruitment. When cell i is recruited after a long delay, typically the input that pushes it across the *go surface* leaves it very close to the *go surface*. This means that cell i experiences a long delay from the firing times of its neighbors, which reset it across the *go surface*, until its own firing. We have found that variable delays after *go surface* crossing contribute to a high variability both in the firing times of cells within a bump and in the intervals between successive recruitments when activity propagates.

5.5 Effects of synaptic depression

In this section, we discuss some of the effects that short-term synaptic depression can have on our network. Synapses that display short-term synaptic plasticity are ubiquitous in the central nervous system. Thus it is of interest to know what general effects such synapses may have on the activity patterns of the networks being considered in this study. For synapses that exhibit short-term synaptic plasticity, the synaptic strength is a function of usage. For the depressing synapses that we focus on here, if the synapse is used often because the frequency of the pre-synaptic cell is high, then synaptic strength decreases. Alternatively, if the synapse is used with lower frequency, then the synapse can act with a higher strength. The equations we use to model a depressing synapse are similar to those in [1]. We use variables d_i to keep track of the extent of depression of each synapse, where d_i is governed by

$$d_i' = ([1 - d_i]/\tau_\gamma)H(v_{thresh} - v_i) - (d_i/\tau_\eta)H(v_i - v_{thresh}). \tag{11}$$

The time constants τ_γ and τ_η are the time constants of recovery and depression of the synapse, respectively. Notice that the more time cell i spends in the active state relative to the time it spends in the silent state, the more the synapse depresses and the weaker it becomes. The effect of the variable d_i is incorporated into the equations (7-9) by

exerting an affect on the variable s_i. In particular, without depression, whenever cell i became active, s_i was reset to 1. Now, with depression, whenever cell i becomes active, s_i is reset to the current value of d_i; that is, $s_i = d_i(t_{spike})$. The value $d_i(t_{spike})$ will change depending on how much time cell i spends below and above v_{thresh}.

We conducted several simulations with depressing synapses. There are two primary effects of synaptic depression that we want to highlight. The first is that depression can act as a band pass filter for incoming signals triggering a bump. In the left panel of Figure 16, we transiently increased I_{ext} to cells 9-11 to 0.5 for 50 msec. As can be seen, some neighboring cells are recruited, but very quickly, the activity dies out. When $I_{ext} < 0.02$, it was too low to cause cells 9-11 to oscillate (simulations not shown). Alternatively, in the right panel of Figure 16, we transiently raised I_{ext} to 0.07 for 50 msec and a bump of 7 cells formed. Thus, intermediate strength inputs trigger bump formation. The network filters out overly weak or strong inputs, allowing intermediate strength inputs to have an effect. It is not hard to understand why large inputs do not trigger a bump. With large inputs, the frequency at which cells 9-11 are driven is too high and their synapses depress too quickly. This results in low synaptic strength and the inability to recruit new neighbors or to sustain the activity of those cells already recruited. We note that a network without depression can act only as a high pass filter.

Another effect, which is related to the first, is that synaptic depression allows localized transient excitatory inputs to curtail oscillations. In particular, oscillations can be terminated by inputs that are not too different from the inputs that can initially trigger a bump. In Figure 17, we generated a bump by raising I_{ext} to cells 9-11 to 0.1 for 50 msec. Then at t=200, we again raised I_{ext} to these same cells to 0.125 for 50 msec. As can be seen, this caused activity in the network to end because the strength of the synapses associated with cells 9-11 depressed so much that the cells could not sustain the oscillations of their neighbors. Thus, localized excitatory inputs can act almost as a toggle switch, at times turning "on" the network, and other times turning "off" the network. Note that in a network without depression, the effect of the second dose of excitation would be to cause the bump to recruit more cells.

In Figure 18, we show an example with self-coupling set to zero ($c_0 = 0$) in which the entire network is oscillating. The oscillations are ended by briefly raising I_{ext} to cells 9-11 for 50 msec as before. This result demonstrates that small and localized transient inputs can dramatically change the character of solutions in excitatory networks that exhibit depression. In other studies [9, 13, 17], inputs to the entire network that are synchronizing have been shown to act as a shut off mechanism. Here we note that the mechanism for shut off is a *local* application of excitation, which induces depression. Depression leads to a decrease in synaptic current and finally a *global* end to network activity. Without depression, no such phenomena could occur.

6 Discussion

For bumps to arise, a mechanism is required to sustain activity and a mechanism is needed to keep it localized. The standard means for achieving these constraints has been the imposition of a Mexican hat synaptic architecture, featuring local excitation and long-range inhibition. This work illustrates an alternative to the Mexican hat and thus broadens our understanding of what ingredients are truly necessary for bumps to exist. More specifically, previous studies had already shown how activity can be sustained without local excitatory connections [17, 18], given a thalamic coupling pattern, which still features long-range inhibition to block the spread of activity. The existence of bumps in a purely excitatory model neuronal network presented here indicates that long-range inhibition is not necessary to keep activity localized, as also recently noted by Drover and Ermentrout [3].

The work in [3] is closely related to ours in the sense that both studies show how to create localized activity patterns in purely excitatory networks. There are some fundamental differences in the systems considered and the techniques used in these two studies, however. In their paper, Drover and Ermentrout concentrate on Type II neurons and analyze temporally periodic, spatially uniform (non-localized) solutions, as well as traveling waves, using a normal form associated with a sub-critical Hopf Bifurcation. They also simulate localized activity, and to achieve this, they require the cells in their underlying network to be bistable between an oscillatory and rest state. In our network, intrinsic neuronal dynamics are Type I rather than Type II, which affects the transition to spiking. Notably, we do not require bistability in the intrinsic description of each cell. Indeed, we choose parameters such that in the absence of input, each cell is at rest. The temporal dynamics of synaptic coupling also play a key role in the bump formation that we have investigated. Specifically, the persistence of bumps in our model results from a combination of desynchrony within the bump and the slow decay of synaptic excitation. The desynchrony provides a way to lower the effective amount of excitation any cell outside of the bump can receive. The slow decay of excitation serves to provide residual excitation to each cell within the bump, placing each cell closer to the *go curve* or *go surface*, and thus in a better position to remain in the bump. An important aspect of our work is the establishment of a geometric criterion, via the *go curve*/*go surface*, which determines whether cells are recruited into the bump or not. An advantage of this approach is that it sheds light on the importance of the timing of synaptic inputs to individual cells and how timing affects the network's ability to create localized activity patterns.

In our model, we included the term c_0 to represent self-coupling. We found that it was much easier to form bumps when $c_0 > 0$. The reason for this is straightforward: self-coupling gives cells that have already fired a boost toward firing again due to the additional residual excitation that it provides during their time in the silent phase.

We note that the self-coupling term could be replaced by any depolarization-activated inward current, such as a high-threshold calcium current (e.g. I_{CaL}) [12].

In previous models of bumps with or without Mexican hat synaptic connectivity, transient excitatory input that induced synchronization would terminate network activity [9, 13, 17]. In the excitatory network that we have studied, in the absence of synaptic depression, excitatory inputs always promote activity. With depression, however, depending on the size or frequency of the input, network activity may grow or may be reduced. In fact, even localized excitatory inputs can terminate widespread network activity (Figure 18), allowing for equally efficient generation and termination of bumps (Figure 17). Thus, networks that include depressing synapses can readily translate different types of inputs into different network outputs. Therefore such networks can effectively be targeted by upstream neurons to perform tasks associated with rate or temporal coding. For example, as shown in Figure 16, only inputs of intermediate strengths activate a bump. Intermediate strength inputs could result from upstream neurons firing at intermediate frequencies (rate code) or from an appropriate number of upstream neurons fired closely enough in time to initiate an intermediate strength input (temporal code).

In closing, we note that a commonly used experimental means for assessing the role of some component in a complex system is to eliminate that component and observe the changes that result. Here, we carried out a computational and analytical version of this approach, with regard to the role of inhibition in the generation and sustainment of localized activity in a network of bursting Type I cells. The non-robustness of the resulting structures, which our analysis demonstrates to be a fundamental property of such solutions to the model equations, suggests that the presence of some inhibition may very well be crucial in networks in which there is a need to generate activity patterns of precise sizes in the presence of noise. In networks where more transient, less precisely tuned manifestations of localized activity suffice, the presence of inhibition may be less important, at least if the neurons themselves exhibit the right (Type I) dynamics. In particular, the thresholding properties of such dynamics desynchronize cells coupled with synaptic excitation [4], which can curtail the spread of activity in a network without inhibition.

7 Appendix

The system (1) used for simulations includes the intrinsic currents $I_{Ca} = g_{Ca} m_\infty(v)(v - E_{Ca}), I_K = g_K w(v - E_K)$, and $I_L = g_L(v - E_L)$. In this model, parameters and variables are scaled such that the physiologically relevant range of voltages is a subset of the interval $[-0.5, 0.5]$. Also, the synaptic equation is modified to take the form $s' = \alpha[1 - s]H(v - v_{thresh}) - \beta s H(v_{thresh} - v)$, so that s really does approach 1 when $v > v_{thresh}$, as

discussed in Section 4, even for finite α. The voltage-dependent functions in the system are $m_\infty(v) = .5(1+\tanh((v+.01)/.15)), w_\infty(v) = .5(1+\tanh((v-.05)/.15)), 1/\tau_w(v) = (0.6-0.3H(v+.4))\cosh((v-.05)/.3)$, where $H(v) = 1$ if $v \geq 0$ and $H(v) = 0$ otherwise. The parameter values used in all simulations, unless other specified, are listed in the following table. Note that only the relative sizes of these parameters are important, and thus we omit units.

parameter	value	parameter	value	parameter	value
g_{Ca}	1.1	E_{Ca}	1.0	I_{ext}	0.075
g_K	2.0	E_K	-0.7		
g_L	0.5	E_L	-0.5		
$\bar{g}_{syn}$	1.0	E_{syn}	0.5	c_0	0.02
c_1	0.022	c_2	0.006	c_3	0.001
α	5	β	0.072	v_{thresh}	0.2

For Figures 16-18, the same parameters as above were used except for the following: $\beta = 0.08$, $c_1 = 0.026$, $c_2 = .0015$, $\tau_\gamma = 10.5$, $\tau_\eta = 1$, $\bar{g}_{syn} = 1.2$.

Acknowledgments: Our primary interest in the problem considered in this paper was sparked by a talk given by Bard Ermentrout at a workshop in March 2003 at the Mathematical Biosciences Institute at Ohio State University. We thank the organizers of the MBI workshop for their support. This work was also supported, in part, by grants DMS-0108857 (JR) and DMS-0315862 (AB) from the National Science Foundation.

References

[1] A. Bose, Y. Manor, and F. Nadim. Bistable oscillations arising from synaptic depression. *SIAM J. Appl. Math.*, **62**:706–727, 2001.

[2] N. Brunel. Dynamics and plasticity of stimulus-selective persistent activity in cortical network models. *Cereb. Cortex*, **13**:1151–1161, 2003.

[3] J. Drover and B. Ermentrout. Nonlinear coupling near a degenerate Hopf (Bautin) bifurcation. *SIAM J. Appl. Math.*, **63**:1627–1647, 2003.

[4] B. Ermentrout. Type I membranes, phase resetting curves, and synchrony. *Neural Comput.*, **8**:979–1001, 1996.

[5] B. Ermentrout. *Simulating, Analyzing, and Animating Dynamical Systems*. SIAM, Philadelphia, 2002.

[6] B. Ermentrout and J. Rinzel. Reflected waves in an inhomogeneous excitable medium. *SIAM J. Appl. Math.*, **56**:1107–1128, 1996.

[7] G. Ermentrout. Neural nets as spatio-temporal pattern forming systems. *Reports on Progress in Physics*, **61**:353–430, 1998.

[8] G. Ermentrout and N. Kopell. Parabolic bursting in an excitable system coupled with a slow oscillation. *SIAM J. Appl. Math.*, **46**:233–253, 1986.

[9] B. Gutkin, C. Laing, C. Chow, G. Ermentrout, and C. Colby. Turning on and off with excitation: the role of spike-timing asynchrony and synchrony in sustained neural activity. *J. Comput. Neurosci.*, **11**:121–134, 2001.

[10] D. Hansel and H. Sompolinsky. Modeling feature selectivity in local cortical circuits. In C.Koch and I. Segev, editors, *Methods in Neuronal Modeling: From Ions to Networks*, pages 499–567. The MIT Press, Cambridge, MA, second edition, 1998.

[11] F. Hoppensteadt and E. Izhikevich. *Weakly Connected Neural Networks*. Springer-Verlag, New York, Berlin, and Heidelberg, 1997.

[12] D. Johnson and S. Wu. *Foundations of cellular neurophysiology*. The MIT Press, Cambridge, MA, 1995.

[13] C. Laing and C. Chow. Stationary bumps in networks of spiking neurons. *Neural Comp.*, **13**:1473–1494, 2001.

[14] C. Morris and H. Lecar. Voltage oscillations in the barnicle giant muscle fiber. *Biophys. J.*, **35**:193–213, 1981.

[15] R. Osan, J. Rubin, and B. Ermentrout. Regular traveling waves in a one-dimensional network of theta neurons. *SIAM J. Appl. Math.*, **62**:1197–1221, 2002.

[16] J. Rinzel and G. Ermentrout. Analysis of neural excitability and oscillations. In C.Koch and I. Segev, editors, *Methods in Neuronal Modeling: From Ions to Networks*, pages 251–291. The MIT Press, Cambridge, MA, second edition, 1998.

[17] J. Rubin, D. Terman, and C. Chow. Localized bumps of activity sustained by inhibition in a two-layer thalamic network. *J. Comput. Neurosci.*, **10**:313–331, 2001.

[18] J. Rubin and W. Troy. Sustained spatial patterns of activity in neuronal populations without recurrent excitation. *SIAM J. Appl. Math*, 2004.

[19] P. Sharp, H. Blair, and J. Cho. The anatomical and computational basis of the rat head-direction cell signal. *Trends Neurosci.*, **24**:289–294, 2001.

[20] J. Taube. Head direction cels and the neurophysiological basis for a sense of direction. *Prog. Neurobiol.*, **55**:225–256, 1998.

[21] X.-J. Wang. Synaptic reverberation underlying mnemonic persistent activity. *Trends Neurosci.*, **24**:455–463, 2001.

Figure Captions

Figure 1. Stable bumps. LEFT: The grayscale encodes the v values of cells in a 20 cell network with parameters from the Appendix. Time evolves from top to bottom, with different cells' voltage traces appearing in different vertical columns in the plot. Time steps of .0025 time units were used, and values of v were only plotted once every 25 time steps. Although we only show the first 1250 time units, this bump remained stable for 10000 simulation time units. RIGHT: This plot is similar to the one on the left except that $c_0 = 0.025, c_1 = 0.0253, c_2 = 0.003, c_3 = 0.001$ and the bump may be metastable.

Figure 2. Gradual recruitment with variable delays. Protocols for simulation and plotting were similar to Figure 1. LEFT: $c_0 = 0.025, c_1 = 0.0253, c_2 = 0.003, c_3 = 0.001$, and a shock of $I_{ext} = 2.0$ was applied to cells 9-11 for 100 time units. RIGHT: $c_0 = 0.02, c_1 = 0.025, c_2 = 0.003, c_3 = 0.002$ and a shock of $I_{ext} = 0.2$ was applied to cells 9-11 for 50 time units. In both cases, activity continued to spread gradually after the times shown here.

Figure 3. A bump of 8 cells in a ring of 20 theta neurons. This bump persists indefinitely. Note that the greyscale encodes the synaptic variable s associated with each cell, which remains at 0 for inactive cells.

Figure 4. The phase circle for the theta model (2) with $b < 0$. The arrowheads show the direction of flow generated by equation (2) on the circle.

Figure 5. The $\theta - g_{isyn}$ phase plane. The solid curve $\mathcal{P}$ consists of critical points of (3) with $\beta = 0$, given by equations (4), for different values of g_{isyn}. Note that the critical points coalesce at $g_{isyn} = -b = 1/3$ (dotted line). The points $(\theta_S, 0), (\theta_U, 0)$ are actual critical points of the (θ, g_{isyn}) system from (3) for any β. The dashed curve is a branch of the stable manifold of $(\theta_U, 0)$. The thin solid curves show trajectories starting from $(-1.5, 0.2), (-1.5, 0.4), (-1.5, 0.6)$, respectively. Initially, $d\theta/dt > 0$ along these curves.

Figure 6. Recruitment in the $\theta - g_{isyn}$ phase plane. The trajectory of a cell that eventually is recruited into the bump is shown (solid). It receives many synaptic inputs, each characterized by a rapid increase in the $g_{i_{syn}}$ value, before it is eventually reset above the *go curve* (dotted).

Figure 7. Nullclines for system (5). LEFT: With $I_{ext} = 0$, the v- and w-nullclines intersect in three points, labeled with asterisks. RIGHT: Increasing I_{ext} raises the v-nullcline, eliminates two intersections of the nullclines, and allows for the existence of a periodic orbit (with direction of flow indicated by the arrows).

Figure 8. The parabola P in $(v, g_{i_{syn}})$-space, defined from the intersections of the slice $w = w_l$ with different v-nullclines corresponding to different values of $g = g_{i_{syn}}$ (here denoted by g).

Figure 9. The flow in $(v, g_{i_{syn}})$-space with $w = 0.02$, $w' = 0$, and $g'_{i_{syn}} = -\beta g_{i_{syn}}$. This numerically generated figure shows the parabola $\mathcal{P}$ (densely dotted curve), the *go curve* (dashed curve) corresponding to a branch of the stable manifold of the saddle point $(v_{c_m}, 0)$, and several trajectories. The trajectories were obtained from the flow from initial conditions $(v, g_{i_{syn}}) = (-0.4, 0.01), \ldots, (-0.4, 0.06)$. Note that $dv/dt > 0$ along these curves, as long as they remain above $\mathcal{P}$. A trajectory from one of these initial points escapes from the silent phase if and only if the initial condition lies above the *go curve*.

Figure 10. The flow (with $w' = 0$) from various labeled points in $(v, g_{i_{syn}})$-space. Dotted lines denote jumps due to instantaneous synaptic inputs. Solid curves denote trajectories ensuing after jumps. Here we have taken $t_{ap} = 0$, such that $g'_{i_{syn}} < 0$ at all times outside of jumps, to simplify the illustration. See text for definition of points A-F.

Figure 11. Phase space for system (10). The critical point $(v_m, w_m, 0)$ has a 2-dimensional stable manifold, which we denote W^s. By definition, this is invariant under the flow of (10). For any fixed w, this flow can be projected to the $(v, g_{i_{syn}})$-plane, and the corresponding *go curve* for this projection is given by the intersection of W^s with the plane of constant w. As an example, one such curve is shown (dashed line) for $w = w_{RK}$, the w-value at the right (upper) knee of the v-nullcline with $g_{i_{syn}} = 0$.

Figure 12. Crossing the *go curve* determines escape from the silent phase. LEFT: The trajectory of a cell in the $(v, g_{i_{syn}})$-plane, before and during its recruitment into a bump. The stars (*) along the trajectory demarcate equal time intervals of 1 time unit each. RIGHT: A blow up of the part of the trajectory that determines recruitment. The dashed, dotted, and dash-dotted curves are *go curves* that are relevant for three different inputs; see text.

Figure 13. Once a cell crosses the *go curve*, no subsequent synaptic input is required for the cell to fire. Bold arrows indicate direction of flow. The bold trajectory is the same one shown in Figure 12, although we have now included a segment of the trajectory corresponding to return from the silent phase from the active phase (marked with the leftward arrow) to illustrate that both trajectories shown really do make it to the active phase. The dash-dotted bold trajectory shows the result of the same simulation but with all subsequent inputs to the cell blocked, starting from a moment just after the cell crosses the *go curve* associated with $t = t_9 + t_{ap}$.

In particular, the cell does not feel the tenth input, which arrives when the cell's position in the plane corresponds to the arrow labeled "shut off". The cell is still able to escape from the silent phase.

Figure 14. Trajectories of a recruited cell (dashed) and its non-recruited neighbor (solid) projected into the $(v, g_{i_{syn}})$-plane. The dotted curves are *go curves* for the two cells at particular moments in time. The leftmost curve is the *go curve* for the recruited cell when it gets recruited. The rightmost curve is an arbitrarily selected *go curve* for the non-recruited cell. At any fixed time, the non-recruited cell's trajectory lies below the corresponding *go curve*, but the trajectory approaches quite close to the relevant *go curves*.

Figure 15. $g_{i_{syn}}$ versus time for the same recruited (dashed) and non-recruited (solid) cells shown in Figure 14. The dotted line at $g_{i_{syn}} \approx .027$ corresponds to the value of $g_{i_{syn}}$ at recruitment of the recruited cell. Although $g_{i_{syn}}$ for the non-recruited cell exceeds this value several times in the simulation shown, the cell is not recruited.

Figure 16. Filtering properties with depression. Depression allows only intermediate strength inputs to initiate bumps. LEFT: The input $I_{ext} = 0.5$ to cells 9-11 is so high that the synapses from these cells depress too quickly to recruit cells. No bump forms. RIGHT: The input $I_{ext} = 0.07$ to cells 9-11 is in an intermediate range where it is able to initiate a bump. Simulation for smaller values of I_{ext} for which no bump formed are not shown.

Figure 17. Toggling with synaptic depression. Networks that have depressing synapses can turn "on" and "off" with similar transient excitatory inputs. The network is turned "on" at $t = 0$ with $I_{ext} = 0.1$ to cells 9-11 for 50 msec. It is turned "off" by raising I_{ext} to 0.125 to these same cells from 200 to 250 msec.

Figure 18. Localized inputs have global effects. The simulation demonstrates how transient inputs to small numbers of cells can have a global impact on network activity patterns. The parameter I_{ext} was raised to 0.3 for cells 9 to 11 from $t = 100$ to 125 msec. This resulted in the end of the network activity. The simulation also shows a curious phenomenon associated with networks that have depressing synapses. They can exhibit transient changes in bump size due to the strengthening and weakening of synapses.

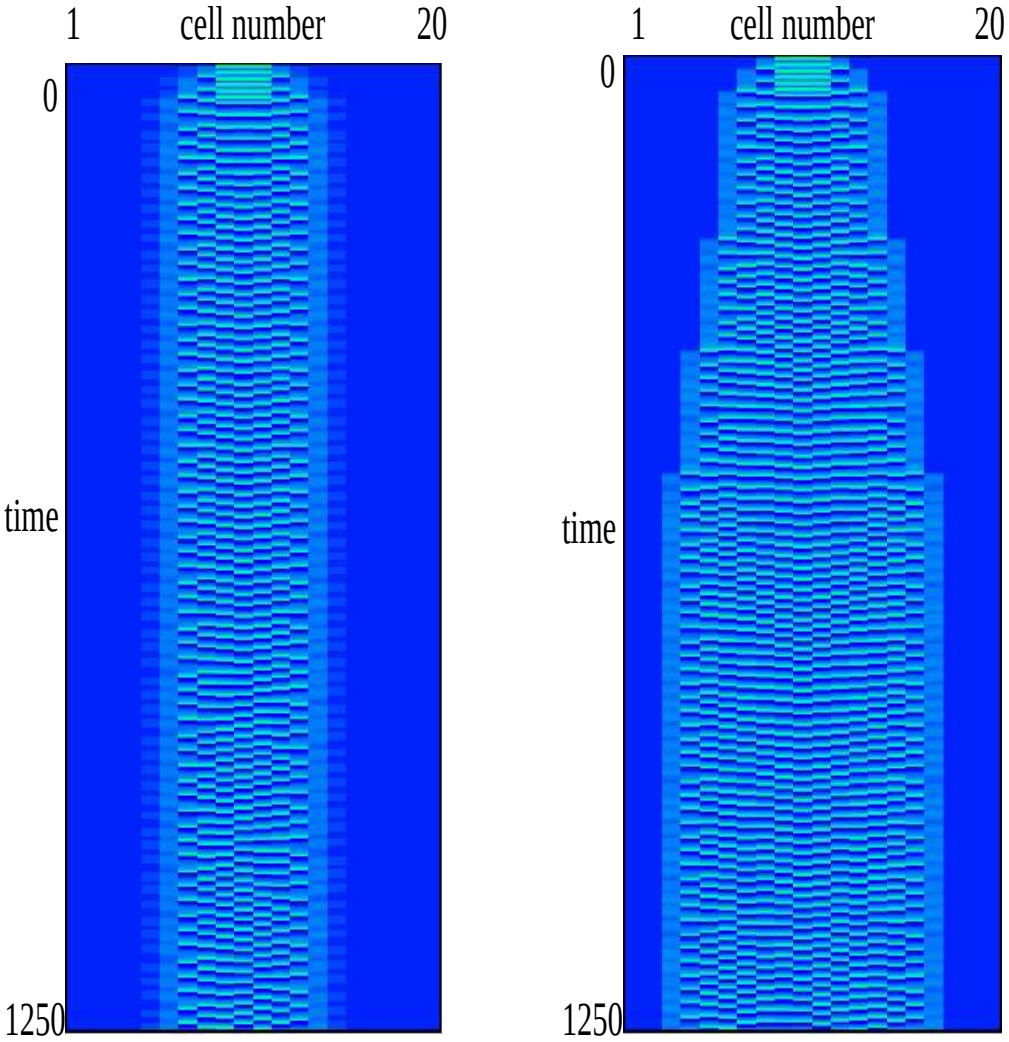

Figure 1: Stable bumps. LEFT: The grayscale encodes the v values of cells in a 20 cell network with parameters from the Appendix. Time evolves from top to bottom, with different cells' voltage traces appearing in different vertical columns in the plot. Time steps of .0025 time units were used, and values of v were only plotted once every 25 time steps. Although we only show the first 1250 time units, this bump remained stable for 10000 simulation time units. RIGHT: This plot is similar to the one on the left except that $c_0 = 0.025, c_1 = 0.0253, c_2 = 0.003, c_3 = 0.001$ and the bump may be metastable.

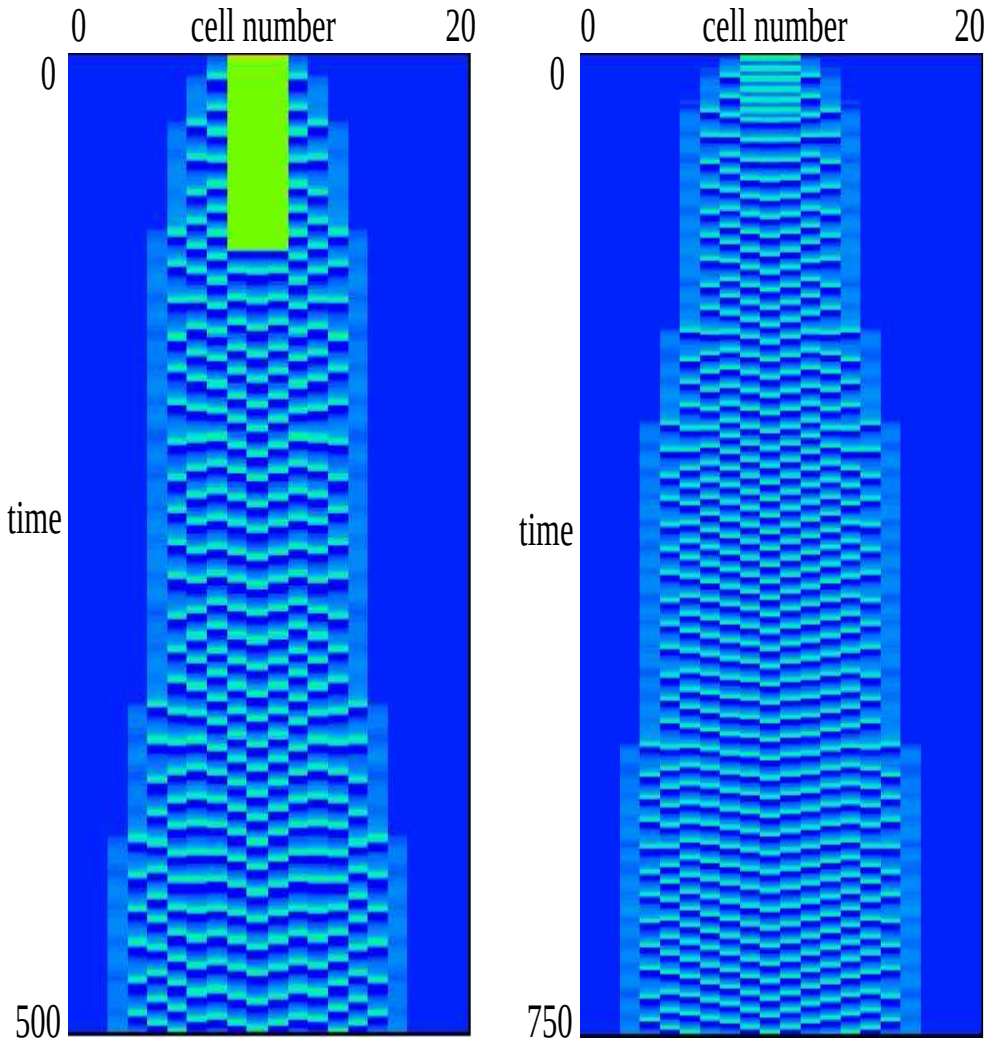

Figure 2: Gradual recruitment with variable delays. Protocols for simulation and plotting were similar to Figure 1. LEFT: $c_0 = 0.025, c_1 = 0.0253, c_2 = 0.003, c_3 = 0.001$, and a shock of $I_{ext} = 2.0$ was applied to cells 9-11 for 100 time units. RIGHT: $c_0 = 0.02, c_1 = 0.025, c_2 = 0.003, c_3 = 0.002$ and a shock of $I_{ext} = 0.2$ was applied to cells 9-11 for 50 time units. In both cases, activity continued to spread gradually after the times shown here.

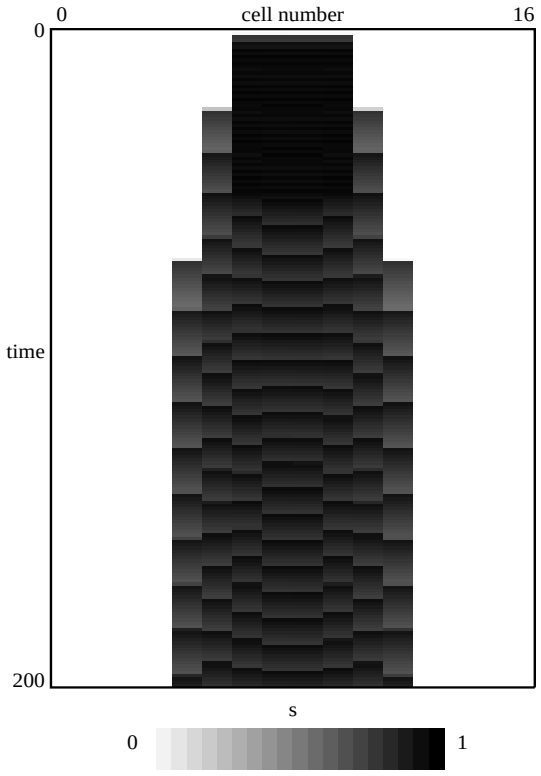

Figure 3: A bump of 8 cells in a ring of 20 theta neurons. This bump persists indefinitely. Note that the greyscale encodes the synaptic variable s associated with each cell, which remains at 0 for inactive cells.

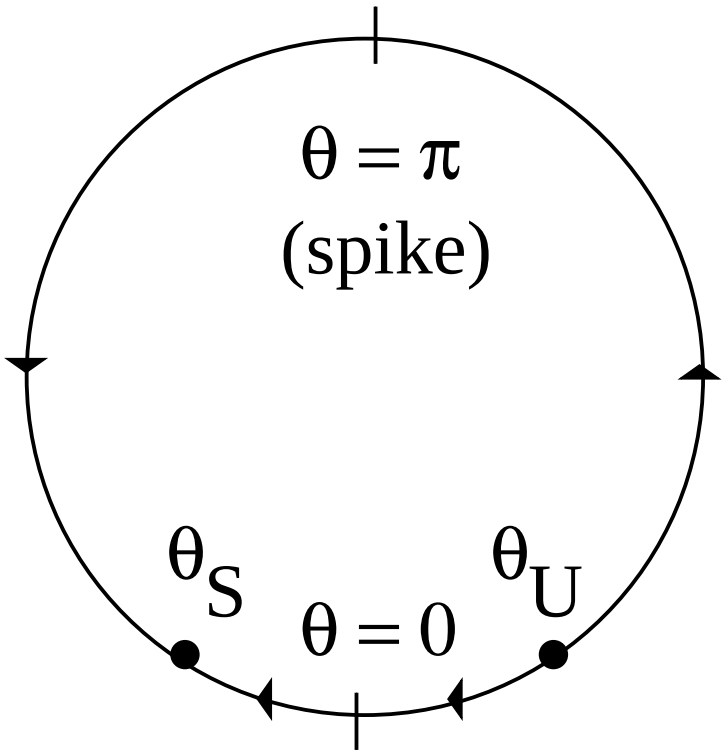

Figure 4: The phase circle for the theta model (2) with $b < 0$. The arrowheads show the direction of flow generated by equation (2) on the circle.

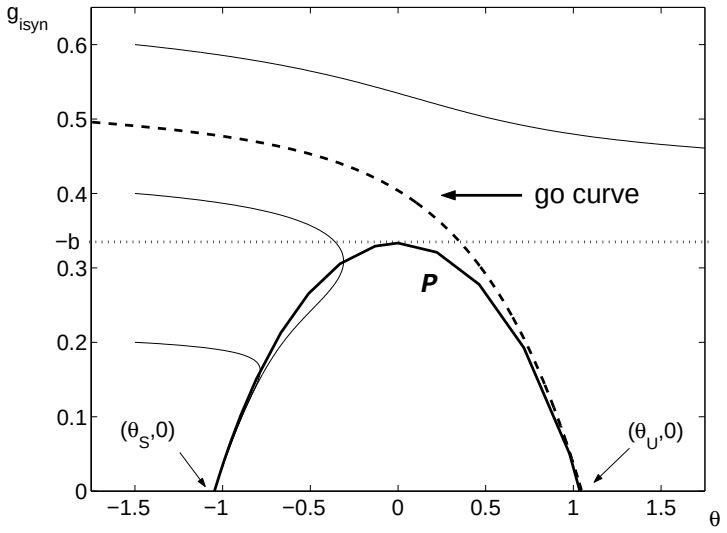

Figure 5: The $\theta - g_{isyn}$ phase plane. The solid curve $\mathcal{P}$ consists of critical points of (3) with $\beta = 0$, given by equations (4), for different values of g_{isyn}. Note that the critical points coalesce at $g_{isyn} = -b = 1/3$ (dotted line). The points $(\theta_S, 0), (\theta_U, 0)$ are actual critical points of the (θ, g_{isyn}) system from (3) for any β. The dashed curve is a branch of the stable manifold of $(\theta_U, 0)$. The thin solid curves show trajectories starting from $(-1.5, 0.2), (-1.5, 0.4), (-1.5, 0.6)$, respectively. Initially, $d\theta/dt > 0$ along these curves.

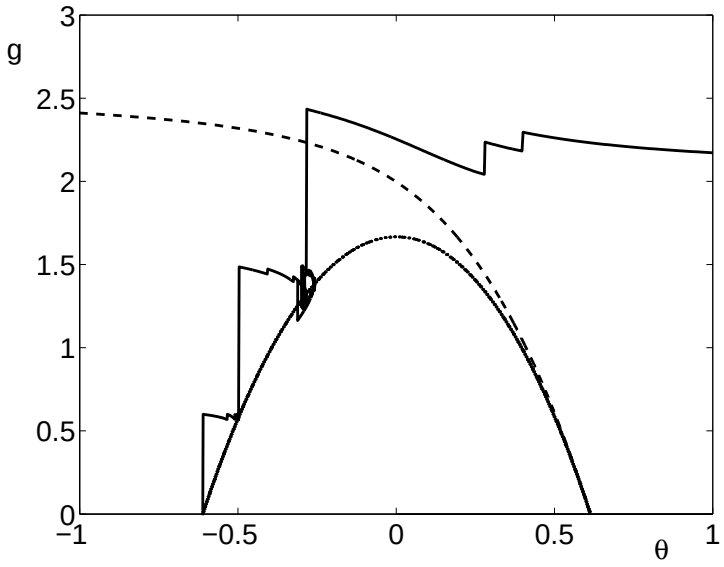

Figure 6: Recruitment in the $\theta - g_{isyn}$ phase plane. The trajectory of a cell that eventually is recruited into the bump is shown (solid). It receives many synaptic inputs, each characterized by a rapid increase in the $g_{i_{syn}}$ value, before it is eventually reset above the *go curve* (dotted).

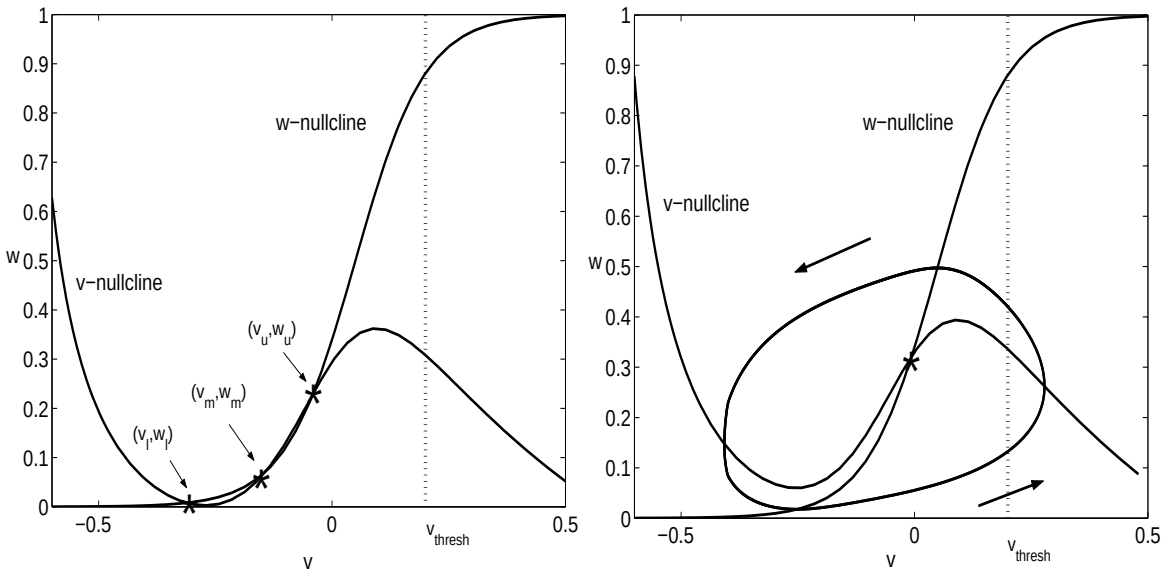

Figure 7: Nullclines for system (5). LEFT: With $I_{ext} = 0$, the v- and w-nullclines intersect in three points, labeled with asterisks. RIGHT: Increasing I_{ext} raises the v-nullcline, eliminates two intersections of the nullclines, and allows for the existence of a periodic orbit (with direction of flow indicated by the arrows).

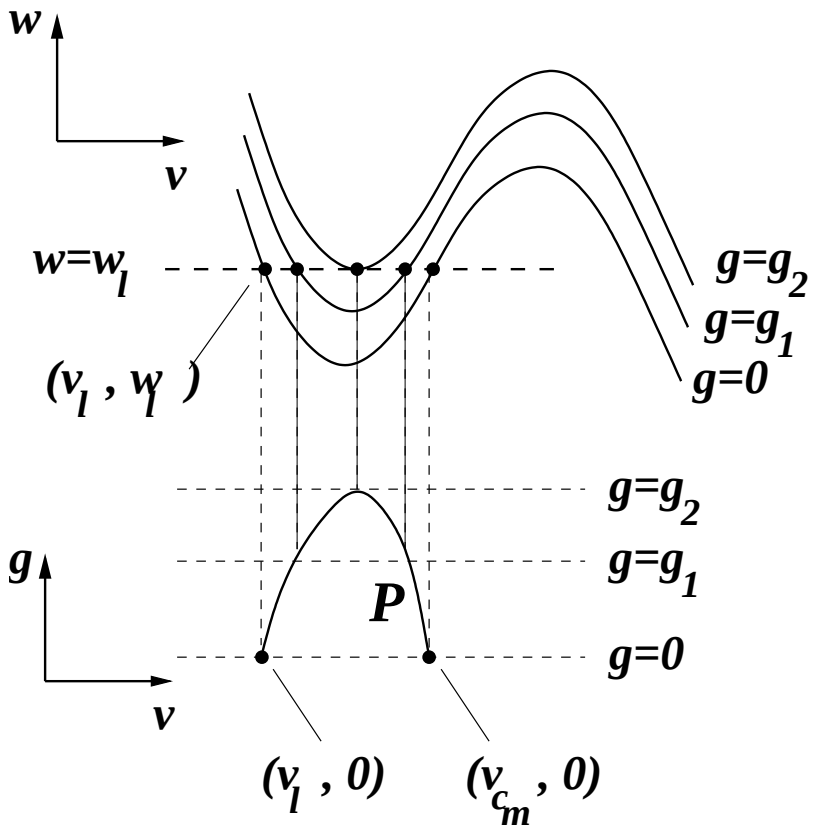

Figure 8: The parabola P in $(v, g_{i_{syn}})$-space, defined from the intersections of the slice $w = w_l$ with different v-nullclines corresponding to different values of $g = g_{i_{syn}}$ (here denoted by g).

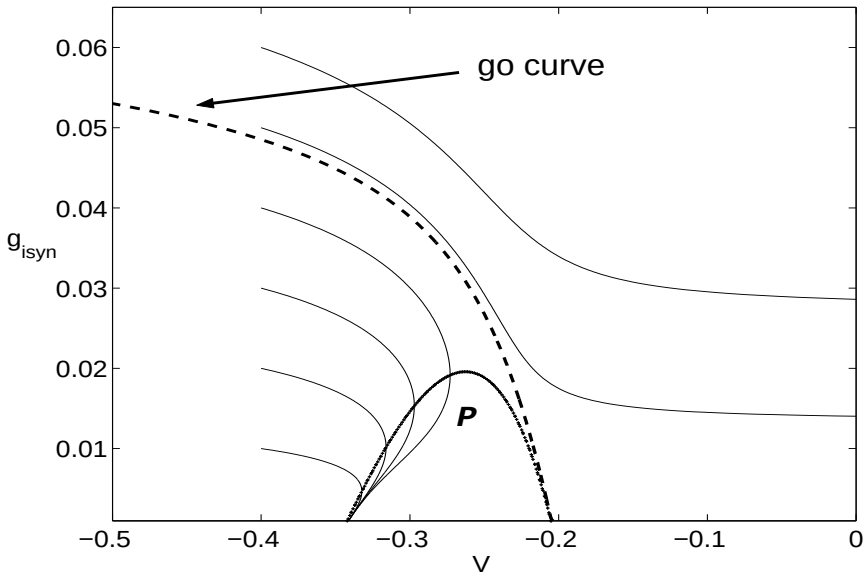

Figure 9: The flow in $(v, g_{i_{syn}})$-space with $w = 0.02$, $w' = 0$, and $g'_{i_{syn}} = -\beta g_{i_{syn}}$. This numerically generated figure shows the parabola $\mathcal{P}$ (densely dotted curve), the *go curve* (dashed curve) corresponding to a branch of the stable manifold of the saddle point $(v_{c_m}, 0)$, and several trajectories. The trajectories were obtained from the flow from initial conditions $(v, g_{i_{syn}}) = (-0.4, 0.01), \ldots, (-0.4, 0.06)$. Note that $dv/dt > 0$ along these curves, as long as they remain above $\mathcal{P}$. A trajectory from one of these initial points escapes from the silent phase if and only if the initial condition lies above the *go curve*.

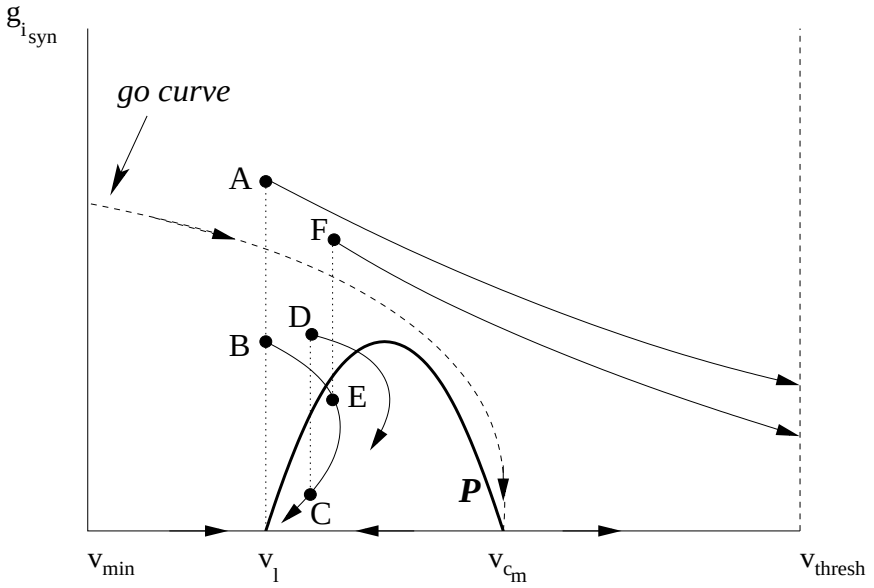

Figure 10: The flow (with $w' = 0$) from various labeled points in $(v, g_{i_{syn}})$-space. Dotted lines denote jumps due to instantaneous synaptic inputs. Solid curves denote trajectories ensuing after jumps. Here we have taken $t_{ap} = 0$, such that $g'_{i_{syn}} < 0$ at all times outside of jumps, to simplify the illustration. See text for definition of points A-F.

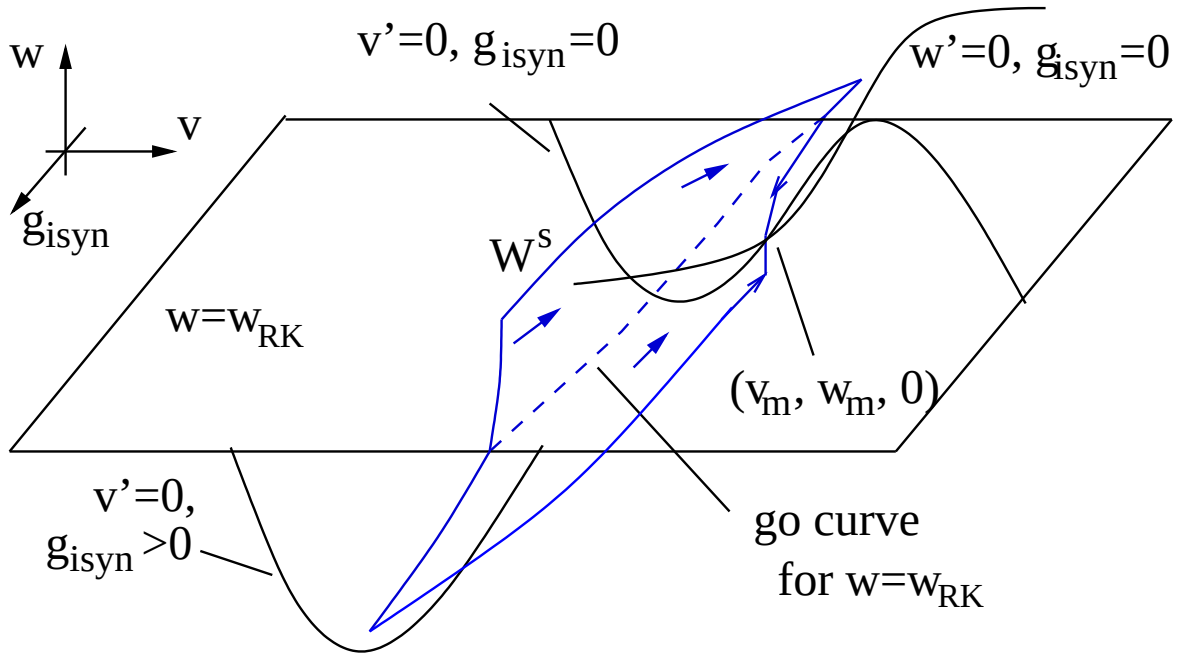

Figure 11: Phase space for system (10). The critical point $(v_m, w_m, 0)$ has a 2-dimensional stable manifold, which we denote W^s. By definition, this is invariant under the flow of (10). For any fixed w, this flow can be projected to the $(v, g_{i_{syn}})$-plane, and the corresponding *go curve* for this projection is given by the intersection of W^s with the plane of constant w. As an example, one such curve is shown (dashed line) for $w = w_{RK}$, the w-value at the right (upper) knee of the v-nullcline with $g_{i_{syn}} = 0$.

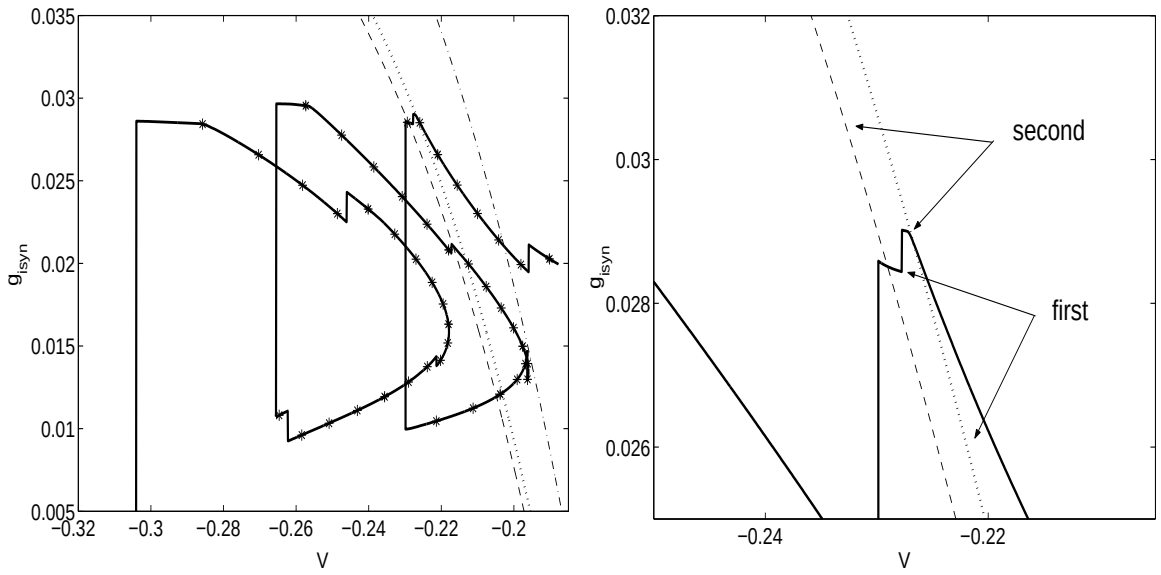

Figure 12: Crossing the *go curve* determines escape from the silent phase. LEFT: The trajectory of a cell in the $(v, g_{i_{syn}})$-plane, before and during its recruitment into a bump. The stars (*) along the trajectory demarcate equal time intervals of 1 time unit each. RIGHT: A blow up of the part of the trajectory that determines recruitment. The dashed, dotted, and dash-dotted curves are *go curves* that are relevant for three different inputs; see text.

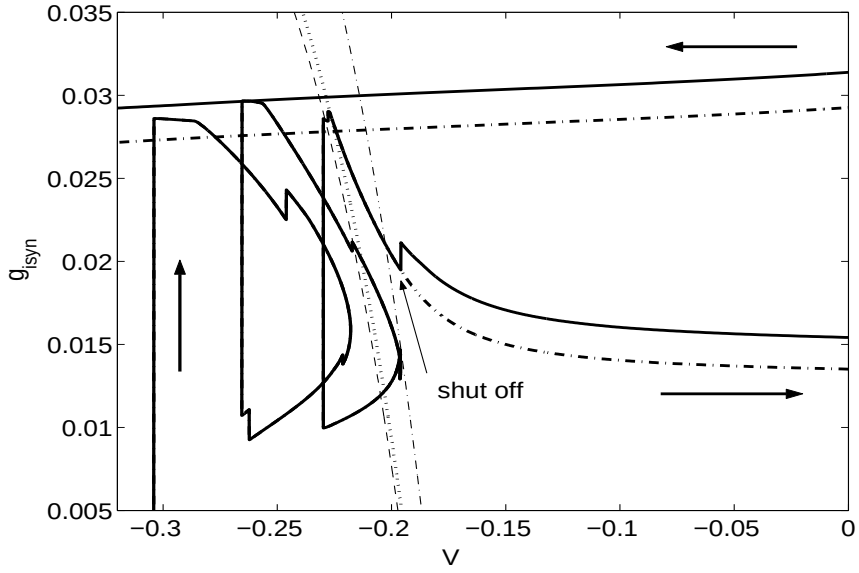

Figure 13: Once a cell crosses the *go curve*, no subsequent synaptic input is required for the cell to fire. Bold arrows indicate direction of flow. The bold trajectory is the same one shown in Figure 12, although we have now included a segment of the trajectory corresponding to return from the silent phase from the active phase (marked with the leftward arrow) to illustrate that both trajectories shown really do make it to the active phase. The dash-dotted bold trajectory shows the result of the same simulation but with all subsequent inputs to the cell blocked, starting from a moment just after the cell crosses the *go curve* associated with $t = t_9 + t_{ap}$. In particular, the cell does not feel the tenth input, which arrives when the cell's position in the plane corresponds to the arrow labeled "shut off". The cell is still able to escape from the silent phase.

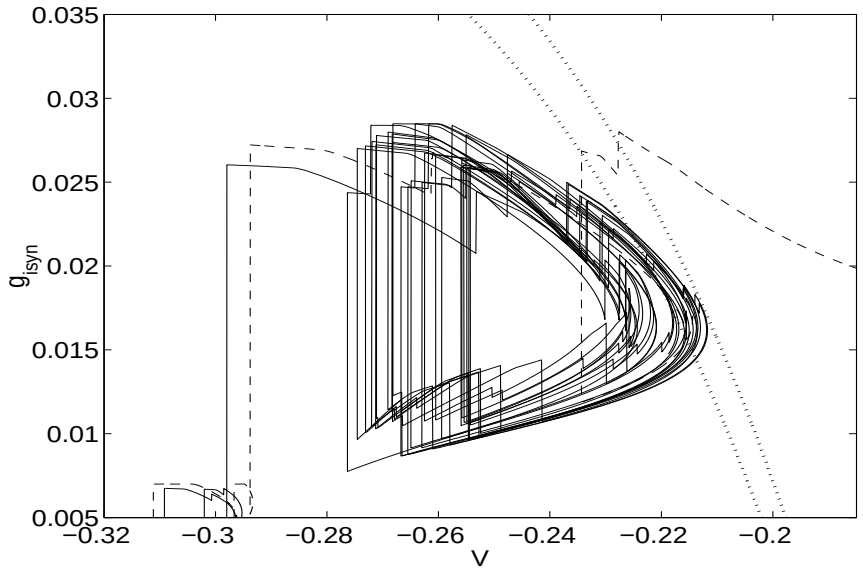

Figure 14: Trajectories of a recruited cell (dashed) and its non-recruited neighbor (solid) projected into the $(v, g_{i_{syn}})$-plane. The dotted curves are *go curves* for the two cells at particular moments in time. The leftmost curve is the *go curve* for the recruited cell when it gets recruited. The rightmost curve is an arbitrarily selected *go curve* for the non-recruited cell. At any fixed time, the non-recruited cell's trajectory lies below the corresponding *go curve*, but the trajectory approaches quite close to the relevant *go curves*.

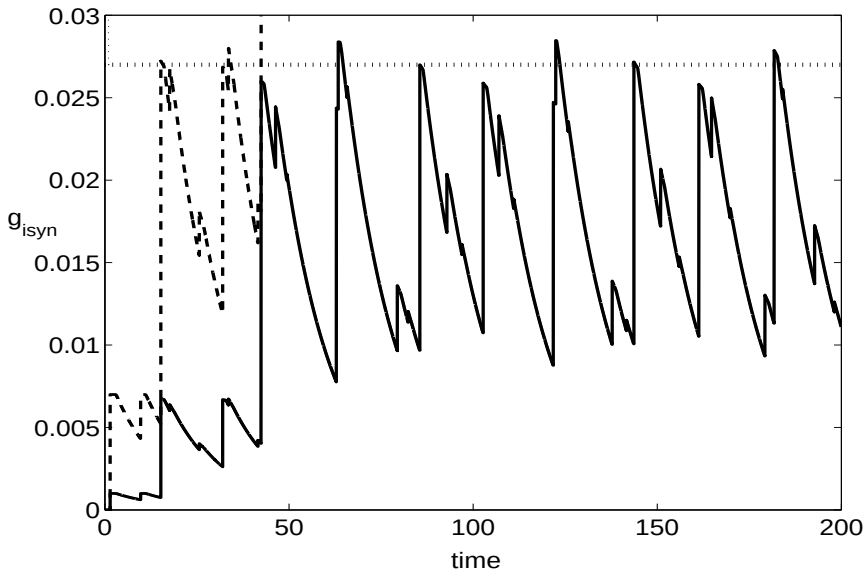

Figure 15: $g_{i_{syn}}$ versus time for the same recruited (dashed) and non-recruited (solid) cells shown in Figure 14. The dotted line at $g_{i_{syn}} \approx .027$ corresponds to the value of $g_{i_{syn}}$ at recruitment of the recruited cell. Although $g_{i_{syn}}$ for the non-recruited cell exceeds this value several times in the simulation shown, the cell is not recruited.

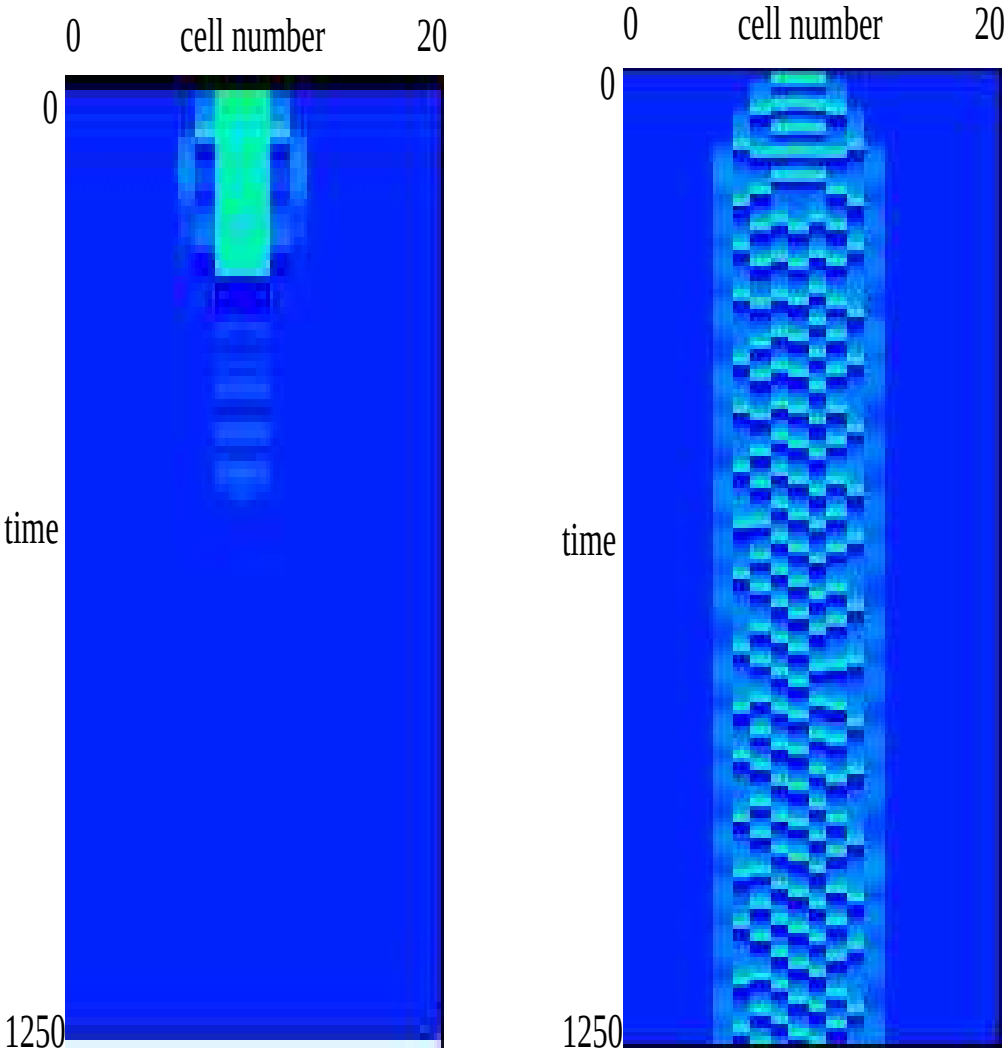

Figure 16: Filtering properties with depression. Depression allows only intermediate strength inputs to initiate bumps. LEFT: The input $I_{ext} = 0.5$ to cells 9-11 is so high that the synapses from these cells depress too quickly to recruit cells. No bump forms. RIGHT: The input $I_{ext} = 0.07$ to cells 9-11 is in an intermediate range where it is able to initiate a bump. Note that initial conditions for this simulation were asymmetric, leading to the asymmetry in the bump. Simulation for smaller values of I_{ext} for which no bump formed are not shown.

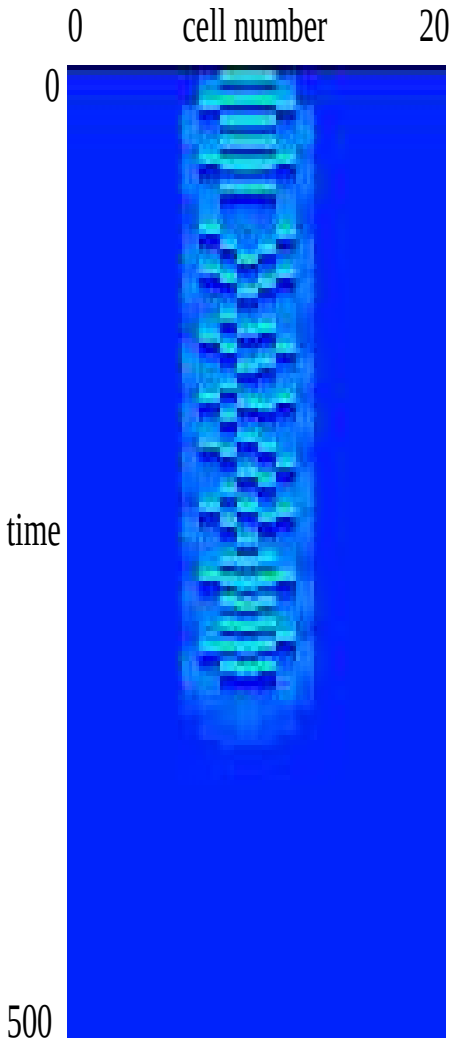

Figure 17: Toggling with synaptic depression. Networks that have depressing synapses can turn "on" and "off" with similar transient excitatory inputs. The network is turned "on" at $t = 0$ with $I_{ext} = 0.1$ to cells 9-11 for 50 msec. It is turned "off" by raising I_{ext} to 0.125 to these same cells from 200 to 250 msec.

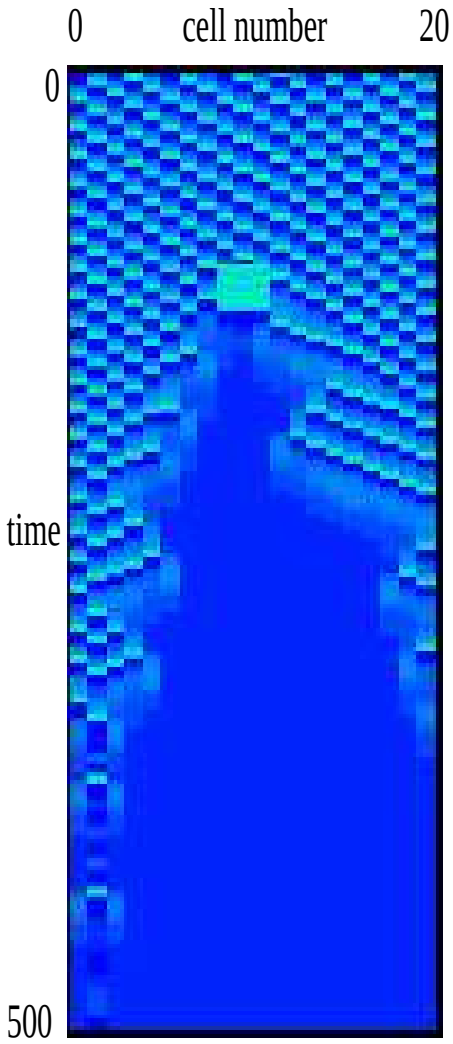

Figure 18: Localized inputs have global effects. The simulation demonstrates how transient inputs to small numbers of cells can have a global impact on network activity patterns. The parameter I_{ext} was raised to 0.3 for cells 9 to 11 from $t = 100$ to 125 msec. This resulted in the end of the network activity. The simulation also shows a curious phenomenon associated with networks that have depressing synapses. They can exhibit transient changes in bump size due to the strengthening and weakening of synapses.